Accepted Manuscript

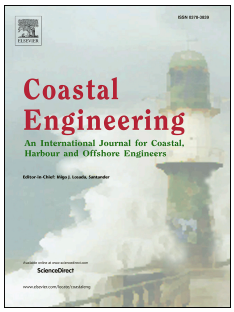

Numerical modelling of the flow and bed evolution of a single bore-driven swash event on a coarse sand beach

Riccardo Briganti, Nicholas Dodd, Giorgio Incelli, Gustaaf Kikkert

PII: S0378-3839(18)30099-1

DOI: 10.1016/j.coastaleng.2018.09.006

Reference: CENG 3426

To appear in: *Coastal Engineering*

Received Date: 7 August 2017

Revised Date: 19 July 2018

Accepted Date: 29 September 2018

Please cite this article as: Briganti, R., Dodd, N., Incelli, G., Kikkert, G., Numerical modelling of the flow and bed evolution of a single bore-driven swash event on a coarse sand beach, *Coastal Engineering* (2018), doi: https://doi.org/10.1016/j.coastaleng.2018.09.006.

Numerical modelling of the flow and bed evolution of a single bore-driven swash event on a coarse sand beach.

Riccardo Briganti,[a], Nicholas Dodd,[a], Giorgio Incelli,[b], Gustaaf Kikkert,[c]

[a] *Coastal Dynamics and Engineering Group, Nottingham Transportation Engineering Centre, Faculty of Engineering, University of Nottingham, Nottingham NG7 2RD, U.K.*
[b] *Hydraulic Modelling Team, Pick Everard, Leicester LE1 1HA, UK*
[c] *Jacobs NZ Ltd, Hamilton, 3204, New Zealand*

Abstract

This paper examines the numerical prediction of the sediment transport and bed evolution for a single swash event on a coarse sediment beach. In these conditions bed load is the dominant mode of sediment transport. Laboratory experiments of a single bore-driven swash event are simulated numerically using a fully-coupled model that solves the system of Non Linear Shallow Water Equations and the Exner sediment conservation formula. The analysis focuses on two aspects: the optimal choice of parameters for the Meyer-Peter and Müller sediment transport formula and the model used for computing the shear stress. The methods tested for the bed shear stress are the momentum integral method and the Chezy formulation in which the friction factor is computed using two different formulae. Infiltration into the beach and its effects on the shear stress and sediment transport are also modelled. Results show that the basic Meyer-Peter and Müller sediment transport formula provides good results in the run-up. On the other hand, the sediment transport in the early stage of the backwash is overestimated. A reduction of the sediment mobility constant in the formula in the backwash marginally improves the results. However, the causes of the overestimation of the sediment transport at the early stage of the backwash is the overestimation of the shear stress, while at later stages there are several contributions that are identified, i.e. modelling of the sediment transport and infiltration. It is also suggested that the Meyer-Peter and Müller sediment transport formula might not capture the complexity of the processes involved during the backwash. The comparison of the methods for the estimate of the bed shear stress show that comparable results can be obtained using the momentum integral method and the Chezy formulation with time and space varying friction factor. The resulting bed evolution is also described. In the predicted final profile, deposition is found in the upper part of the beach and erosion in the lower part. A bed step is formed just below the position of the initial shoreline. This feature is determined by the onset of an hydraulic jump during the backwash.

Keywords: Swash zone, morphodynamics, bed load, coarse sediment beach.

1. Introduction

Bore-driven swash is an example of boundary layer flows, for which the flow and the sediment bed evolve with the same timescale. This characteristic constitutes one of the most challenging aspects in the understanding of intra-swash processes. Their accurate description depends upon the availability of a detailed description of both the hydrodynamics and sediment transport within a swash cycle itself.

In this contribution we consider a coarse sediment beach, where bed load is the dominant modality of sediment transport. Chardón-Maldonado et al. (2016) show that there is significant evidence that, for these conditions, the Meyer-Peter and Müller (MPM) formula, and in general sediment transport formulae that have an explicit dependence on the cube of the flow velocity, give good quantitative estimates of the intra-swash sediment transport. Adjustment of the calibration constant, as well as the inclusion of a pressure gradient term have been found to slightly increase the accuracy of the prediction in the uprush, and it was suggested that different calibration constants for the uprush and backwash phases may improve the prediction of the sediment transport (Othman et al., 2014).

In the MPM formula the bottom shear stress is computed either using an explicit relationship between the velocity of the flow and the bed shear stress, or by using simple sub-models (e.g. the momentum integral method, Incelli et al., 2016), which use the computed local flow velocity to obtain a value of the shear stress, without using empirical relationships. Neither of the two approaches explicitly accounts for the water depth. Li et al. (2017) proposed to limit the local value of sediment transport based on the idea that the sediment can reach a maximum possible concentration in the water column that corresponds to water filled with sediments. The sediment discharge is therefore computed as the minimum value between this upper limit and that provided by a sediment transport formula. The Li et al. (2017) approach is tested for semi-analytical test cases and for a specific value of the bed mobility parameter in the Grass formula.

The MPM sediment transport formula is very commonly used in numerical models. Among these, wave resolving models based on Non Linear Shallow Water Equations (NLSWE), coupled with the Exner equation for the sediment conservation are able to accurately simulate swash type problems on mobile beds (e.g. Kelly and Dodd, 2009, Briganti et al., 2012, Zhu et al., 2012, Zhu and Dodd, 2013, Hu et al., 2015, Incelli et al., 2016, Postacchini et al., 2012). However, in a recent review of the numerical advances in describing intra-swash processes, Briganti et al. (2016) indicated that when two different formulae, both derived by modifying MPM, are used, the result, in terms of intra-swash bed evolution, can be very different despite similar final bed configurations.

The intra-swash sediment transport measurements of O'Donoghue et al. (2016) allow a detailed comparison between the observed and the modelled sediment transport. This enables us to analyse the quantitative and qualitative agreement between experimental results and numerical prediction, and to identify the

weaknesses and strengths of sediment flux and bed shear stress fomulations on coarse sand beaches in the context of wave resolving models. In this work these aspects are analysed by testing different formulations of the bed shear stress, i.e. the momentum integral and the Chezy methods, and different parameters of the MPM formula. To this end we carry out a sensitivity analysis using established formulations for the bed shear stress and sediment transport. We define various combinations of the most important parameters and test them by simulating the O'Donoghue et al. (2016) experiment. The objective of the paper is to quantify the impact of these parameters on the flow above the beach surface and sediment transport and provide guidance for modelling this type of swash flows.

The paper is organised as follows: after this introduction the laboratory tests are presented in Section 2. Section 3 describes the numerical model. Section 4 describes how the physical processes are modelled in this work, focusing on the validation of the infiltration model, and the presentation of the sub-models for the shear stress and sediment transport. Section 5 presents the results of the sensitivity analysis applied to shear stress and sediment transport formulations. In Section 6, discussion of the results and conclusions are given.

2. Laboratory Tests

The experiments were carried out in the laboratory swash facility at the University of Aberdeen (Scotland,U.K.). O'Donoghue et al. (2016) describe the setup and the experimental results in detail, here only the basic features will be described. The swash facility (Fig. 1) is built into a 20 m long, 0.9 m high and 0.45 m wide, glass-sided flume. The facility consists of a water reservoir placed inside the flume at one end. One of the reservoir walls is actually a gate, which is raised at high speed to produce the dambreak that generates the swash event on a beach with an initial slope of 1:10. In the horizontal part in front of the reservoir, the flume has a fixed bed. Two beaches were tested, a coarse sand beach (measured $D_{50} = 1.3\ mm$) and a gravel beach (measured $D_{50} = 8.4\ mm$). Only the coarse sand beach will be considered here. This is because in gravel beaches the infiltration/exfiltration processes are more complex and deeply influence the sediment stability and transport. This type of analysis is beyond the scope of this paper.

Measurements of the flow bed-parallel and bed-orthogonal velocity components and depth were taken along the beach at five PIV/LIF observation stations referred to as $PIV2$ to 6 (see Fig. 1). The position of the measurement stations is defined in a frame of reference with the x axis parallel to the initial bed and y normal to it. Their cross-shore locations are: $x = 0.072, 0.772, 1.567, 2.377\ m$ and $3.177\ m$. The experiments were designed specifically to measure sediment transport during uprush and backwash, no morphodynamic quantity was measured. To this end two different types of sediment trap, one for the uprush, one for the backwash, were used. Both traps consisted of cages with a metal

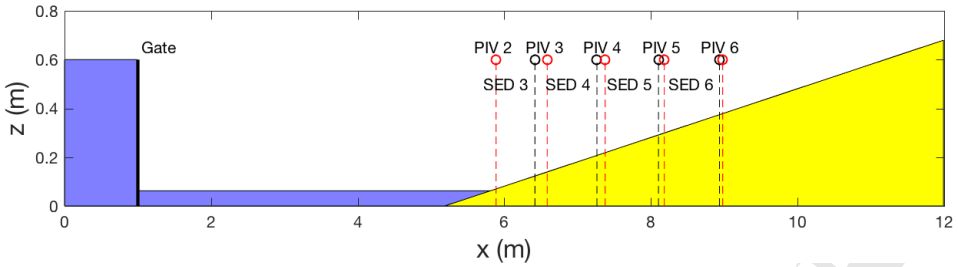

Figure 1: Schematic of the Aberdeen swash facility with the numerical domain used. Also, sediment traps (-Θ-) and the centres of PIV/LIF stations (-Θ-) are indicated.

frame at the opening. The run-up trap faces downslope, and was placed on the beach and quickly lifted. The backwash trap faces upslope and it was quickly lowered to intercept the sediments. In order to obtain measurements along the beach the experiments were repeated and the traps located in a different position. The traps were released at set times in order to obtain a time series of sediment transport rates during the swash event more details are presented in O'Donoghue et al., 2016). Also, the experiments were repeated several times to obtain an average value of the transport rates. The locations of the traps coincide with the offshore limit of the PIV/LIF measurement areas. In the following the traps are indicated using the abbreviation SED followed by the number of the PIV/LIF station to which they are associated.

3. Numerical Model

3.1. Introduction

The numerical model is based on the NLSWE coupled with the Exner equation for the bed evolution. The NLSWE, written in conservative form, reads:

$$\frac{\partial h}{\partial t} + \frac{\partial hU}{\partial x} = -w_{inf} \tag{1}$$

$$\frac{\partial hU}{\partial t} + \frac{\partial \left(hU^2 + \frac{1}{2}gh^2\right)}{\partial x} = -gh\frac{\partial z_B}{\partial x} - \frac{\tau_{b,inf}}{\rho}. \tag{2}$$

Here x is the abscissa, t is time, U denotes the depth-averaged horizontal velocity, h is the local water depth, z_B is the bed level, g is the gravitational acceleration, $\tau_{b,inf}$ is the bottom shear stress computed including the effect of the infiltration; we use the notation τ_b to indicate the shear stress computed without considering the effect of infiltration; ρ is the water density, and w_{inf} is the infiltration flux of the water percolating into the permeable beach and it is considered positive downward. The momentum exchange between the flow above the beach and that within it has been neglected for the following reason.

As argued in Pokrajac (2013), this term is equal to the product of infiltration flux (i.e., discharge per unit plan area of the bed) and the average streamwise velocity at the level of the surface-subsurface interface. Between the grain crests and the surface/subsurface interface (assumed to be around the middle of the top layer of grains) the majority of the flow streamwise velocity has already been absorbed by the grains (hence generating bed shear stress), so the remaining streamwise momentum, i.e. the momentum transferred to the subsurface, has negligible magnitude. We have checked this assumption by running preliminary simulations with and without the momentum exchange term: as expected the inclusion of the momentum term had negligible effect on results.
The Exner equation reads:

$$\frac{\partial z_B}{\partial t} + \xi \frac{\partial q_b}{\partial x} = 0 \tag{3}$$

where $\xi = 1/(1-p)$, p being the bed porosity, and q_b is the instantaneous bed load sediment transport. The system of the NLSWE and Exner equation can be written in vector form:

$$\frac{\partial \mathbf{W}}{\partial t} + \frac{\partial \mathbf{F}(\mathbf{W})}{\partial x} = \mathbf{S}, \tag{4}$$

where $\mathbf{W} = [h, hU, z_B]^T$ is the vector of unknowns, $\mathbf{F} = \left[hU, hU^2 + \frac{1}{2}gh^2, \xi q_b\right]^T$ is the flux vector and $\mathbf{S}$ is the vector of the source terms. This includes three contributions: the gravitational, the bed friction and the subsurface term, so that: $\mathbf{S} = \mathbf{S}_g + \mathbf{S}_f + \mathbf{S}_{inf}$, where $\mathbf{S}_g = \left[0, -gh\frac{\partial z_B}{\partial x}, 0\right]^T$ and $\mathbf{S}_f = [0, -\tau_b/\rho, 0]^T$ and $\mathbf{S}_{inf} = [-w_{inf}, 0, 0]^T$ is the source term for the infiltration. No exfiltration or groundwater is considered here, as well air pressure build up in the beach is not modelled, unlike in Steenhauer et al. (2012). When the infiltration front reaches the initial position of the water table $w_{inf} = 0$ is imposed. w_{inf} is computed using the equation

$$w_{inf} = p\frac{\partial \zeta}{\partial t} = k_{inf} I, \tag{5}$$

where ζ is the local infiltration depth, and k_{inf} the hydraulic conductivity of the sediment. I is the hydraulic gradient and it is given by the Darcy-Forchheimer expression :

$$I = a_{inf} w_{inf} + b_{inf} w_{inf}^2, \tag{6}$$

where a_{inf} and b_{inf} are the Forchheimer coefficients. Following Steenhauer et al. (2012), Eq. (6) can be rearranged to write w_{inf} as a function of I, which can be expressed also as $I = (1 + h/\zeta)$. The expression for w_{inf} is:

$$w_{inf} = \frac{1}{2b_{inf}} \left(\sqrt{a_{inf}^2 + 4\left(1 + \frac{h}{\zeta}\right) b_{inf}} - a_{inf} \right). \tag{7}$$

Eq. (7) is used in Eq. (5) to obtain an ordinary differential equation that is solved at each time step to obtain ζ. From this w_{inf} is computed using Eq. (5). Note that Eq. (7) is singular at the beginning of the infiltration process, as initially it is $\zeta = 0$. A priming value for ζ is therefore used, following the approach by Dodd et al. (2008).

3.2. The numerical scheme

Eq. (4) is discretized in space into a set of M computational nodes (equally spaced at a distance Δx). Hence, at a generic time level n, $\mathbf{W}_i^n = \mathbf{W}(i\Delta x, n\Delta t)$; we assume piecewise constant variables between nodes. The system (4) is solved using a TVD-MacCormack scheme. The basic scheme involves two steps:

$$\mathbf{W}_i^{pr} = \mathbf{W}_i^n - \frac{\Delta t}{\Delta x}\left(\mathbf{F}_{i+1}^n - \mathbf{F}_i^n\right) + \Delta t \mathbf{S}_{i+\frac{1}{2}} \tag{8}$$

$$\mathbf{W}_i^{cr} = \mathbf{W}_i^p - \frac{\Delta t}{\Delta x}\left(\mathbf{F}_i^n - \mathbf{F}_{i-1}^n\right) + \Delta t \mathbf{S}_{i-\frac{1}{2}} \tag{9}$$

These two steps are combined to give a solution at the next time step:

$$\mathbf{W}_i^{n+1} = \frac{1}{2}\left(\mathbf{W}^{pr_i} + \mathbf{W}^{cr_i}\right) \tag{10}$$

The scheme is second order in time and space and can be equipped with total variation diminishing (TVD) properties by modifying (10), to provide the solution at the next time step

$$\mathbf{W}_i^{n+1} = \frac{1}{2}\left(\mathbf{W}^{pr_i} + \mathbf{W}^{cr_i}\right) + \frac{\Delta t}{\Delta x}\left(\mathbf{D}_{i+\frac{1}{2}}^n - \mathbf{D}_{i-\frac{1}{2}}^n\right) \tag{11}$$

Note that $\mathbf{S}$ is computed at $(i+\frac{1}{2})\Delta x$ at the predictor stage and at $(i-\frac{1}{2})\Delta x$ in the corrector stage, to preserve the C-property of the scheme. Details of the TVD function $\mathbf{D}$ are found in Incelli et al. (2016).

3.3. Numerical Set-up

The numerical domain used in this study is the whole University of Aberdeen swash facility shown in Fig. 1. The distance between two computational nodes is $\Delta x = 0.01\ m$. The model was run with constant Courant Number $C = 0.8$. A general description of the domain and physical parameters used in the numerical simulations is shown in Table 1. In all tests the infiltration parameters used in the simulations are those suggested in Steenhauer et al. (2012).

Common physical parameters and numerical settings	
Domain length	12 m
Spatial step size (Δx)	1.0×10^{-2} m
Courant Number (C)	0.8
Reference min water depth (h_{min})	2.0×10^{-3} m
Duration of the simulations	12 s
Bed porosity (p)	0.3
Physical parameters and numerical settings for the coarse sand beach	
Density of water (ρ)	1000 kg/m^3
Relative density of sediment (s_{rel})	2.65
Median sediment diameter (D_{50})	1.3×10^{-3} m
Bed roughness (K_n)	3.0×10^{-3} m
Darcy hydraulic conductivity (k_{inf})	1.3×10^{-2} ms^{-1}
Forcheimer linear coefficient, uprush (a_{inf})	81.2 sm^{-1}
Forcheimer quadratic coefficient (b_{inf})	3.587×10^3 s^{2}m^{-2}

Table 1: Physical parameters and numerical settings used .

4. Modelling of physical processes

In this section we present various methods for modelling the swash bed shear stress and sediment transport. These methods will be used in a sensitivity analysis carried out by a series of tests all simulating the O'Donoghue et al. (2016) experiments.The results of these tests are presented in Section 5. Before introducing the formulations tested for the shear stress and the sediment transport, we validate the modelling of infiltration by carrying out numerical simulations of fixed permeable bed experiments Kikkert et al., 2013.

In this section we also define a particular set of sub-models used for the shear stress and the sediment transport and refer to the resulting model as reference model (RM). This model is intended to have as close a correspondence with reality as possible, i.e. to include all the most relevant processes acting in the case at hand.We also explain the rationale of the sensitivity analysis presented.

4.1. Infiltration.

In this sub-section we assess the modelling of the infiltration process. To do so, we simulate the fixed permeable coarse sand beach experiments presented in Kikkert et al. (2013) so that bed mobility effects on the flow are removed. These experiments share the same beach and generated bore with the experiments presented in Steenhauer et al. (2011) and simulated numerically in Steenhauer et al. (2012). The computation of w_{inf} is carried out via Eq. (7). The computations use the same parameters a_{inf} and b_{inf} as in Steenhauer et al. (2012). In contrast to Steenhauer et al. (2012) the effect of the air flow inside the beach is not modelled.

Results discussed in this sub-section are obtained using τ_b, i.e. without modifications to take into account the effect of infiltration on the shear stress. τ_b was computed using the momentum integral method. While no direct measurements

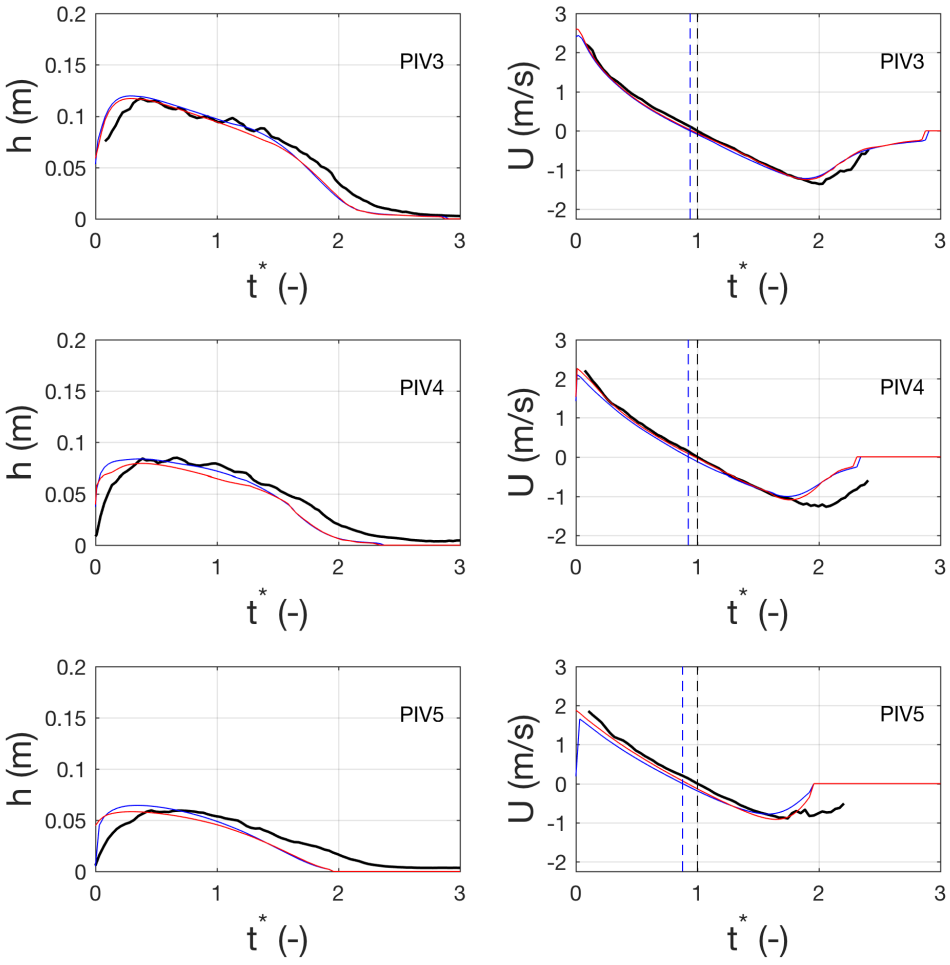

Figure 2: Comparison between numerical and experimental h (left column) and U (right column) at three measurement stations for the Kikkert et al. (2013) experiments on a permeable fixed beach. Experiments (——), numerical results with correction for τ_b (——), results without correction for τ_b (——). t^* for flow reversal in the numerical model (- - -) and in the experiment (- - -) are also indicated.

of w_{inf} are available, the accuracy of the modelling is assessed by comparing

h and U, i.e. the variables describing the flow above the surface of the beach. These are used in computing the bed shear stress and the sediment transport, therefore they are central to this work. Fig. 2 shows h and U for the fixed beach simulation. In this paper time has been normalised using the bore arrival time (t_{ba}) and time of flow reversal (t_{fr}) as measured in the experiments so that the dimensionless time t^* is defined as:

$$t^* = \frac{(t - t_{ba})}{(t_{fr} - t_{ba})} \tag{12}$$

This variable helps in identifying the differences in bore arrival and flow reversal times, which, in the experiments occur at $t^* = 0$ and $t^* = 1$ respectively. Fig. 2 shows that the flow above the beach during the uprush is generally well modelled. The modelled bore arrival time is almost coincident with the experimental one, however h is steeper in the model than in the experiments as a result of the steepening of the free surface typical of NLSWE. The results also reveal that in the uprush U is underestimated, especially in the upper part of the swash lens (see $PIV5$). It is also evident that the modelled flow reversal occurs before experimental flow reversal and backwash is significantly shorter than the experimental backwash; again, this is more evident in the upper swash (note that the time series of measured U at the PIV stations are shorter than the corresponding time series of h). Both issues are the result of neglecting the air compression effect reported in Steenhauer et al. (2011) and modelled in Steenhauer et al. (2012); with the modelled infiltration being faster than the experimental infiltration, the flow above the surface is slightly slower during run-up and the backwash is faster since less water is available above the beach with respect to the experiment. These findings confirm those of Steenhauer et al. (2012), who first identified the role of accounting for the air-compression in the modelling. The modelled w_{inf}, the friction velocity $u_f = \sqrt{\tau_b/\rho}$, and the ventilation parameter, i.e. the ratio $\frac{w_{inf}}{u_f}$ are shown in Fig. 3. In the lower part of the beach, as seen from the results at PIV3 (Fig. 3), the beach saturates during the run-up. The exfiltration occurring at the lower part of the beach at that stage was reported to have very limited influence on the flow during the experiments (Kikkert et al., 2013). In the upper part of the beach infiltration is present in both phases of the swash cycle, with higher infiltration velocities in the uprush. The differences in the saturation of the lower and upper swash explain why the velocity in the upper swash is not modelled as accurately as in the lower part. Once the beach is saturated, the infiltration modelling has no effect on the results. However, since saturation does not occur in the upper swash and effects of the air pressure build-up are present here, results are in worse agreement during the backwash. The value $\frac{w_{inf}}{u_f} = 0.05$, which is important in estimating the effects of infiltration on the shear stress (Conley, 1993) as shown in the next section, is also indicated in Fig. 3. This value is exceeded across the full swash lens during the run-up and, in the upper part of the beach $\frac{w_{inf}}{u_f} < 0.05$ only during late backwash.

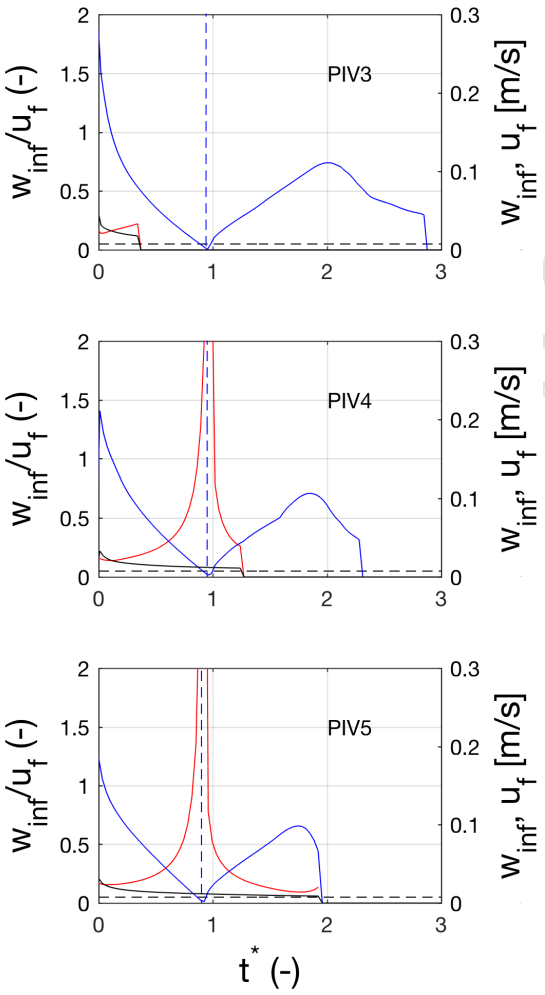

Figure 3: Modelled w_{inf} (——), u_f (——) and ratio w_{inf}/u_f (——) at three PIV stations for the permeable fixed beach of Kikkert et al. (2013). $w_{inf}/u_f = 0.05$ (- - -) and t^* for flow reversal in the numerical model (- - -) are also indicated.

4.2. Bed shear stress.

The models for the computation of the bed shear stress used in the tests are here presented. Before doing so, it is important to recall that an effect of infiltration is to increase the bottom shear stress, due to the 'thinning' of the boundary layer. Neither the momentum integral, or the Chezy formulation, take into account this process. Therefore, a simple model is used to correct the value

of τ_b to take into account the effect of infiltration. The relationship proposed by Conley (1993) for both infiltration and exfiltration is used here. When only infiltration is considered, and noting again that w_{inf} is, in the present model, positive, this relationship is valid for $0 < \frac{w_{inf}}{u_f} < 0.05$ so that an extension of it must be introduced outside this range. The relationship reads:

$$\frac{\tau_{b,inf}}{\tau_b} = \left(1 + \alpha \frac{w_{inf}}{u_f}\right) \qquad \text{if} \quad 0 < \frac{w_{inf}}{u_f} < 0.05 \tag{13}$$

where $\tau_{b,inf}$ is the modified τ_b to account for the infiltration effects and $\alpha = 16$ in the range of w_{inf}/u_f tested by Conley (1993). To apply the Conley adjustment, first w_{inf} is computed using Eq. (5) and τ_b is computed using either the momentum integral or the Chezy method. One of the advantages of the Conley (1993) model is that it can work with any formulation for τ_b.
The modelled $\frac{w_{inf}}{u_f}$, shown in Fig. 3 for the permeable fixed bed case reveals that the parameter exceeds the value of 0.05, i.e. the limit for the validity of Eq. (13) during most of the uprush and the early backwash. $\frac{\tau_{b,inf}}{\tau_b}$ was limited to the value that Eq. (13) assumes for $\frac{w_{inf}}{u_f} = 0.05$, i.e. $\frac{\tau_{b,inf}}{\tau_b} = 1.8$. This value is close to that observed by Kikkert et al. (2013) when comparing the bed shear stresses of the impermeable and permeable fixed coarse sand beaches (shown in the original paper in Fig. 15 and recalled in Fig. 5).
Further numerical tests are also performed to assess the sensitivity of the computation of q_b to different formulations of τ_b. First, we considered the momentum integral method in the form used in Briganti et al. (2011) to which the reader is referred to for more details. Here only the details of how u_f is computed from the depth averaged velocity U are provided in Appendix B. Application of the momentum integral method requires the knowledge of the roughness factor K_n. In the numerical tests this parameter is computed according to the Engelund (1966) model, i.e. $K_n = 2D_{65}$, where $D_{65} = 1.5\ mm$ is the value of the sediment diameter at 65% in the cumulative distribution for the coarse sand used, resulting in $K_n = 0.0030$ m (see Table 1). For the fixed smooth flat bottom in front of the beach $K_n = 0.0001$ m is used. This allows us to compute the friction velocity u_f given h and U. τ_b is computed using the relationship $\tau_b = \rho u_f^2$.
As an alternative to the momentum integral method, the Chezy formulation is used. For the Chezy formulation for which:

$$\tau_b = \frac{1}{2} f_b U \mid U \mid, \tag{14}$$

f_b is computed using two alternative models following the analysis carried out in O'Donoghue et al. (2016): the Swart and the Colebrook formulae. The Swart formula is here written in a form that combines Eq. (6) and (7) in O'Donoghue et al. (2016) and uses the same parametrisation:

$$f_b = 0.0025 \exp\left[5.213 \left(\frac{T_s U_{sd}}{6.27 D_n}\right)^{-0.194}\right], \tag{15}$$

PIV/LIF Station	T_s	U_{Sd}	f_b
$PIV2$	9.86	0.7720	0.0108
$PIV3$	8.60	0.8166	0.0108
$PIV4$	6.82	0.7114	0.0116
$PIV5$	5.63	0.5680	0.0130
$PIV6$	4.15	0.3938	0.0176

Table 2: Parameters used to estimate the friction coefficient according to the Swart formula.

where U_{sd} is the standard deviation of U and T_s is the duration of the swash event at a given location, i.e. $T_s = t_{end} - t_{ba}$. t_{ba} is the time of bore arrival and t_{end} is the time of drying. T_s is computed as the time between the bore arrival and the last available data at each PIV/LIF station, hence the computation is slightly different from O'Donoghue et al. (2016). Table 2 shows the results for f_b at the locations of the PIV stations on the beach. f_b is interpolated linearly between stations and is constant in time.

The Colebrook formula reads:

$$\frac{1}{2\sqrt{f_b}} = -2.0 \log_{10}\left(\frac{K_n}{14.8h} + \frac{2.51}{Re 2\sqrt{f_b}}\right), \tag{16}$$

where $Re = hU/\nu$ is the Reynolds number with ν being the water kinematic viscosity. K_n is determined as in the application of the momentum integral method. With this approach f_b is computed solving the Colebrook formula iteratively at each time step. In order to avoid the singularity at $Re = 0$ a minimum value of $Re = 50$ is used in the computation. This limit has no effect on the prediction of the flow and on the sediment transport as low Re conditions are reached at flow reversal and at the end of the backwash. Caveats on the use of this formula have been stated in O'Donoghue et al. (2016).

4.3. Sediment transport.

Here the MPM formula is used for computing q_b. The original MPM formula reads:

$$q_b(x,t) = \begin{cases} C_s \left(\theta - \theta_{cr}\right)^{\frac{3}{2}} \sqrt{g\left(s_{rel} - 1\right) D_{50}^3} & \theta > \theta_{cr} \\ 0 & \text{Otherwise.} \end{cases} \tag{17}$$

where $\theta = \frac{\tau_b}{\rho g (s_{rel}-1) D_{50}}$ is the Shields parameter, ρ the density of water, D_{50} the median sediment diameter, and s_{rel} is the relative density of the sediment compared to water. θ_{cr} is the critical value of the Shields parameter, C_s is the MPM transport constant. Note that, in Eq. (17), τ_b, i.e. the bed shear stress computed without any correction for the infiltration, is used.

The effects of the infiltration on the sediment transport are usually modelled using a modified Shields parameter (Turner and Masselink, 1998, Nielsen, 1997,

Nielsen et al., 2001) that takes into account the opposing effects of the increase of the shear stress due to 'thinning' of the boundary layer and the stabilising downward flow. Here the formulation proposed in Nielsen (1997) and Nielsen et al. (2001) is used in the form discussed in Baldock and Nielsen (2010) (see Eq. (3) of the paper). This reads:

$$\theta_{inf} = \frac{u_f^2 \left(1 + \alpha \frac{w_{inf}}{u_f}\right)}{g D_{50} \left(s - 1 + \beta \frac{w_{inf}}{w_k}\right)} \tag{18}$$

where w_k is seepage velocity at incipient fluidisation of the sediment, $w_k = k_{inf}(s_{rel} - 1)(1 - p)$, k_{inf} being the Darcy hydraulic conductivity. α and β are two constant values obtained from experiments. α is defined in Eq. (13). The numerator of Eq. (18) takes into account the modification of the shear stress as discussed in the previous subsection, while the denominator models the effect of the downward flow. In this study the effect of the increased stress and downward drag on q_b were studied separately. $\beta = 0.35$ is used as done in Nielsen et al. (2001). When θ_{inf} is used the MPM formula reads:

$$q_b(x,t) = \begin{cases} C_s \left(\theta_{inf} - \theta_{cr}\right)^{\frac{3}{2}} \sqrt{g \left(s_{rel} - 1\right) D_{50}^3} & \theta > \theta_{cr} \\ 0 & \text{Otherwise.} \end{cases} \tag{19}$$

Also, a sensitivity analysis of the value of C_s was carried out. The standard value for the MPM formula is $C_s = 8.0$, however $C_s = 12.0$ is used in (O'Donoghue et al., 2016) and assumed typically in unsteady and oscillatory flows; also $C_s = 22.0$ has been proposed, resulting from the Othman et al., 2014 calibration. All three values are considered in the present work. Othman et al., 2014 also suggested that two different values for C_s, one for the uprush ($C_{s,u}$) and one for the backwash ($C_{s,b}$) could be used. A further set of tests is carried out to assess this option; in these $C_{s,u} = 8.0$ is always used in the uprush and $C_{s,b} < C_{s,u}$ is used for the backwash. $C_{s,b}$ is varied, keeping $C_{s,u} = 8.0$ constant, to carry out a calibration for the best value of $C_{s,b}$.

In the MPM formula the onset of the sediment transport is determined by the Shields parameter reaching a threshold value, the quantitative impact of this threshold, is also investigate by testing $\theta_{cr} = 0$.

Finally, the recent approach by Li et al. (2017) is also tested as an alternative to the MPM. This approach limits the estimate of q_b provided by the Grass formula to an upper limit that corresponds to the maximum possible concentration of sediment in the water column. The Grass formula reads:

$$q_b = A_s U^3 \tag{20}$$

where A_s is the sediment mobility parameter. Eq. (20) does not take into account the role of h. Li et al. (2017) propose the relationship:

$$q_b = min\left(hUc_u, A_s U^3\right), \tag{21}$$

where c_u is the concentration value corresponding to the flow containing the maximum possible sediment, i.e. $c_u = 1 - p$. Note that when q_b is evaluated using Eq. (17) with $\theta_{cr} = 0$ and the Chezy formula, the MPM formula coincides with the Grass formula (Eq. (20)) because the dependence on U^3 is explicit. Following this, the Li et al. (2017) relationship is modified as:

$$q_b = min\left(hUc_u, C_s\theta^{\frac{3}{2}}\sqrt{g\left(s_{rel}-1\right)D_{50}^3}\right), \tag{22}$$

and the equivalent value of A_s is found:

$$A_s = \frac{C_s}{g(s_{rel}-1)}\left(\frac{f_b}{2}\right)^{\frac{3}{2}}. \tag{23}$$

Note that $C_s = 8.0$ is used in Eq. (23) and Eq. (15) to compute f_b.

4.4. Reference model and summary of options tested

We here define the RM that will be used in the next sections and summarise the different options tested. The RM makes use of Eq. (13) to calculate $\tau_{b,inf}$ starting from τ_b computed using the momentum integral method. The calibration parameter in Eq. (13) is $\alpha = 16$ for $0 < \frac{w_{inf}}{u_f} < 0.05$, outside this range the ratio $\tau_{b,inf}/\tau_b = 1/8$ is used. The same values of α are used for all models unless otherwise stated. $\tau_{b,inf}$ is then used in Eq. (2). Also, we compute θ_{inf} by Eq. (18). Here $\beta = 0.35$ is used in all the tested models unless otherwise stated and, using the set of parameters shown in Table 1, $w_k = 0.014$ ms^{-1}. We use θ_{inf} n Eq. (19). $C_s = 8.0$ is used as it is the standard value for the MPM formula. Finally z_B is computed by solving Eq. (3).

Table 3 summarises the parameters used in the model options tested. Each of the model tested uses a set of parameters that varies only parameters that describe one of the processes at play, with respect to the RM. Model 2 does not include corrections for τ_b and θ_{inf}, i.e. does not take infiltration in account in sediment transport modelling. Model 3 does not include a correction for θ_{inf} to take into account the down-flow, i.e. $\beta = 0$, but includes the correction for τ_b (i.e. α is determined with the Conley formula). Model 4 and 5 test the Chezy formulation with f_b found with the Swart and Colebrook formulae respectively. Model 6 to 8 test the different parameters in the MPM formula. Finally Model 9 tests Li et al. (2017) approach using Eq. (22) as an alternative to the MPM.

As a measure of the accuracy of model predictions The Normalised Root Mean Squared Error (ϵ) is used. ϵ at a measuring station is defined as:

$$\epsilon = \frac{\sqrt{\frac{1}{N}\sum_{i=1}^{N}\left(y_{meas,i} - y_{num,i}\right)^2}}{\max(y_{meas}) - \min(y_{meas})}, \tag{24}$$

where N is the number of samples, i is an integer index, y_{meas} is a generic quantity measured at the considered location and y_{num} is the same quantity predicted by the model. The denominator is the range of the measured values at the considered location.

5. Numerical Results

5.1. Sensitivity of hydrodynamics to the modelling of the infiltration effects on τ_b.

As done for the fixed bed experiments, the sensitivity of the modelled h and U to the inclusion of the effects of infiltration on τ_b is assessed. Fig. 4 shows h and U obtained with the RM and without the correction for the infiltration (Model 2); results are very close. Very close results are also obtained in the fixed impermeable bed case, see Fig. 2 in which the results obtained using $\tau_{b,inf}$, i.e. with Eq. (13), are reported to show that mobility of the bed does not contribute to the very close prediction of h and U between the two methods. Also, in both cases the use of $\tau_{b,inf}$ shows no obvious improvement in the prediction of the flow variables compared to using τ_b. Note that in the mobile bed case the effect of neglecting air-compression is less pronounced than in the fixed bed case, although both the slightly slower run-up and shorter backwash are present.

Experimental data of the shear stress are not available for the mobile bed case. Recall that the stresses in both the impermeable and permeable fixed bed experiments of Kikkert et al. (2012) and Kikkert et al. (2013) were computed using the log-law starting from the measured velocities; this operation is not possible for the mobile bed tests. For this reason the stresses computed with and without Eq. (13) are compared with measured bottom shear stress for the impermeable and permeable fixed bed experiments (see Fig. 5). At $PIV3$ the correction is increasing bed shear stress at the early stage of the run-up. A distinctive feature of the numerical $\tau_{b,inf}$ is a jump in the value of the stress that is seen in the run-up in the lower part of the swash (see $PIV3$ in Fig. 5) and in the backwash further up the beach (see $PIV4$ in Fig. 5). This jump occurs at the point of saturation of the beach and it is generated by the sharp change in the Conley formula as w_{inf} becomes naught. While in the model the effect of the infiltration, until the beach saturates, is clearly visible, the data do not show a similar increase. On the contrary, at $PIV3$, a slight reduction of measured stress for the permeable beach compared to the impermeable beach, as a possible consequence of exfiltration at this location (Kikkert et al., 2013). At PIV4 the modelled values of $\tau_{b,inf}$ are all at the upper bound of the stress from the experiments during the uprush and underestimate the stress at $PIV4$ in the early backwash. At $PIV5$, the agreement between the modelled and experimental values is similar to $PIV4$. In the backwash there are very few data for the permeable fixed beach, which seems to indicate that the effect of the infiltration on the stress is reduced. The quality of the agreement between numerical and experimental values is similar, with and without the use of Eq. (13). Independently from both location and correction for the infiltration, the model overestimates backwash shear stress immediately after flow reversal, and it is underestimated at a later stage.

Table 3: Summary of the parameters used in tested modelling options.

Model	$\tau_{b,inf}$	τ_b	q_b	θ_{inf}	θ_{cr}	C_s
RM	Eq. (13)	Momentum Integral	Eq. (19)	Eq. (18)	0.036	8.0
Model 2	Eq. (13) $\alpha = 0$	Momentum Integral	Eq. (19)	Eq. (18) $\beta = 0$	0.036	8.0
Model 3	Eq. (13)	Momentum Integral	Eq. (19)	Eq. (18) $\beta = 0$	0.036	8.0
Model 4	Eq. (13)	Eq. (14) with Eq. (15)	Eq. (19)	Eq. (18)	0.036	8.0
Model 5	Eq. (13)	Eq. (14) with Eq. (16)	Eq. (19)	Eq. (18)	0.036	8.0
Model 6	Eq. (13)	Momentum Integral	Eq. (19)	Eq. (18)	0.0	8.0
Model 7 (a,b)	Eq. (13)	Momentum Integral	Eq. (19)	Eq. (18)	0.036	(a) 12.0, (b) 22.0
Model 8	Eq. (13)	Momentum Integral	Eq. (19)	Eq. (18)	0.036	$C_{s,u}/C_{s,b}$ variable
Model 9	Eq. (13)	Eq. (14) with Eq. (15)	Eq. (22)	Eq. (18) $\beta = 0$	0.0	8.0

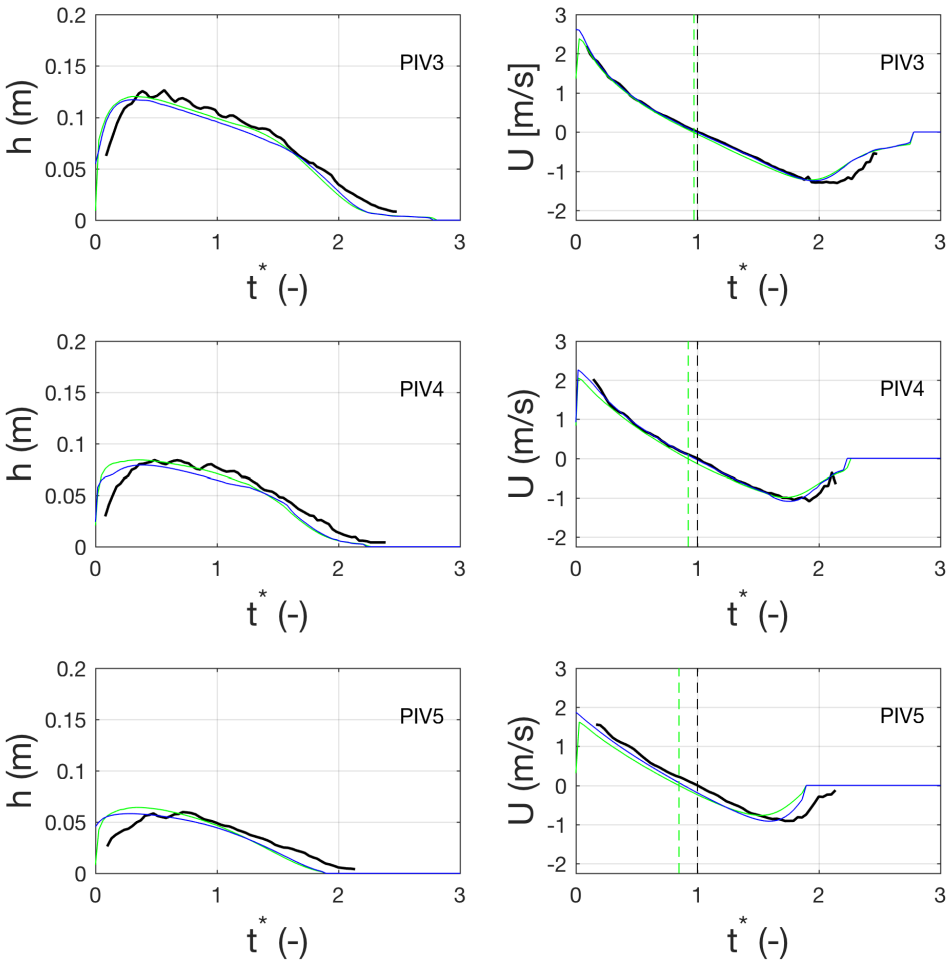

Figure 4: Comparison between numerical and experimental h (left column) and U (right column) at three measurement stations for the O'Donoghue et al. (2016) experiments on a mobile beach. Experiments (——), numerical results with RM (——) and Model 2 (——). t^* for flow reversal in the RM (- - -) and in the experiment (- - -) are also indicated.

5.2. Sensitivity of sediment transport to the modelling of the infiltration downward force.

Here the results from the RM are compared with Model 3, which uses Eq. (18) with $\beta = 0$, to assess the effect of the downward flow. Fig. 6 shows the

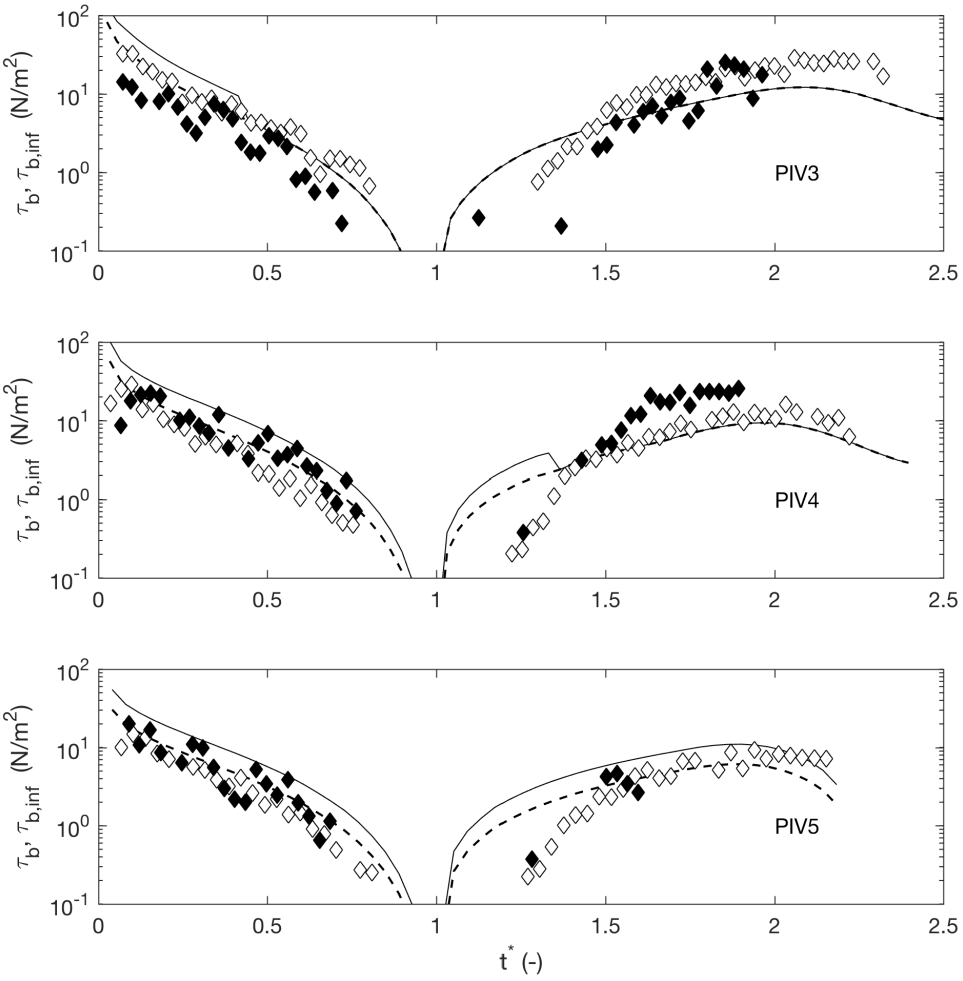

Figure 5: Comparison between $\tau_{b,inf}$ from RM (——) and τ_b from Model 2 (- - -) computed for the mobile beach of O'Donoghue et al. (2016) and the log-law based measurements of τ_b for the impermeable fixed coarse sand beach experiment of Kikkert et al. (2012) (◇) and the permeable fixed coarse sand beach experiment of Kikkert et al. (2013) (◆)

comparison between measured and modelled q_b. Note that the averages of the modelled values of q_b were calculated using the sediment trap release times.

Once t^* is used, the modelled and experimental times at which the averages are plotted might not coincide because the model has slightly different flow re-

versal times than the experiments. As expected the effect of taking into account the downward flow is larger in the uprush, where w_{inf} is larger at both $PIV3$ and $PIV4$. In $PIV5$, where infiltration is present during the whole swash cycle, the effect of the downward flow is noticeable in the downrush as well. Note that at $SED5$ the effect of the reduction of the duration of the backwash in the model compared to the experiments is very evident for q_b as, after $t^* = 1.8$, no flow is present, while sediment transport was still measured.

5.3. Sensitivity of hydrodynamics to τ_b models

The influence of the model used to compute τ_b on the flow variables h and U is assessed by comparing the results of the RM, which uses the momentum integral method, with Model 4 and 5, which use the Chezy formulation with the Swart and Colebrook formulae for f_b respectively. Fig. 7 shows this comparison. In all cases the bore height and the water depth during the uprush are accurately modelled at $PIV3$, while at $PIV4$ and $PIV5$, the bore height is overestimated when the Swart and Colebrook models are used for f_b. All models for τ_b produce an underestimation of h during the backwash. As for U, the three models give very similar results in the uprush, although the Swart and Colebrook models produce a slight underestimation of U with respect to the momentum integral, and in part of the backwash.The level of accuracy of the results is comparable to that obtained with similar solvers (e.g., in Briganti et al., 2016) using the analogous experiments carried out on fixed bed in Kikkert et al. (2012).

Model differences are more evident for U and towards the late stage of the backwash. The Chezy formulation with the Colebrook f_b and momentum integral results are very similar. In all cases the flow in the model slows down less rapidly than in the experiment, at $PIV5$. Fig. 8 shows the differences in predicted $\tau_{b,inf}$ (i.e. the value of τ_b after the correction for infiltration is applied) and the corresponding values of f_b. Note that for the Colebrook and Swart models f_b is that computed by Eq. (16) and Eq. (15) respectively, while for the momentum integral method f_b is back-calculated using the relationship $f_b = \frac{\tau_{b,inf}}{0.5\rho U^2}$. Although it is not possible to assess the accuracy of the prediction of $\tau_{b,inf}$ or f_b, as in the fixed bed case, this plot is useful to identify the relative differences between the models and to better understand the results for q_b. The figure shows that in the uprush $\tau_{b,inf}$ is higher for the Colebrook and Swart models, explaining the slower flow, while in the backwash the momentum integral and Colebrook models predict very similar $\tau_{b,inf}$. The friction coefficients for the Colebrook and Swart models are very similar for most of the swash cycle. f_b computed using the Swart method is constant throughout the swash cycle, while the one computed with the Colebrook model increases at flow reversal and at the late stage of the backwash. f_b back-calculated using the momentum integral is highest at bore arrival but is very close to the value computed by the Colebrook model for the rest of the uprush. The spike at bore arrival is due to the fact that U is initially small as the bore arrives and rapidly transitions to the highest value within the swash cycle. In the backwash the three models diverge, with the momentum integral computing a much higher f_b after flow reversal ($\tau_{b,inf}$ remains higher than the Colebrook estimate at this stage of the

flow) with respect to the other two estimates. In the late backwash f_b for both the Colebrook and momentum integral models is higher than the constant value computed by the Swart formula, explaining the different results for h and U for the three models at this stage.

In Table 4 ϵ for the prediction of h and U at different PIV stations is shown for all the numerical tests carried out and discussed subsequently (see Sections 5.4 and 5.5).

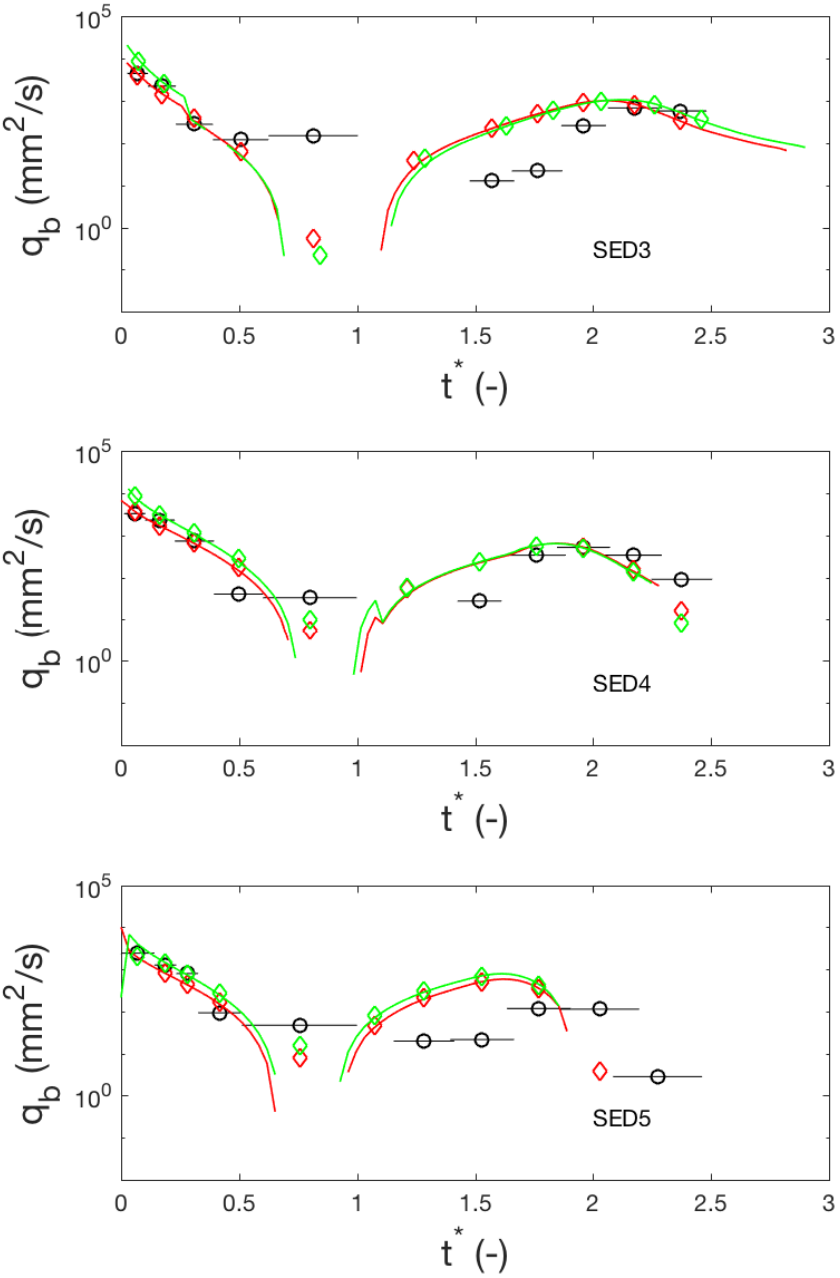

Figure 6: Comparison between measured and modelled q_b at three sediment traps. q_b measured by the traps averaged over the trap release intervals (○) and trap release interval (——). Numerical prediction, diamonds, averages over the traps release intervals. Prediction with Model 3 (——) and prediction with RM (——).

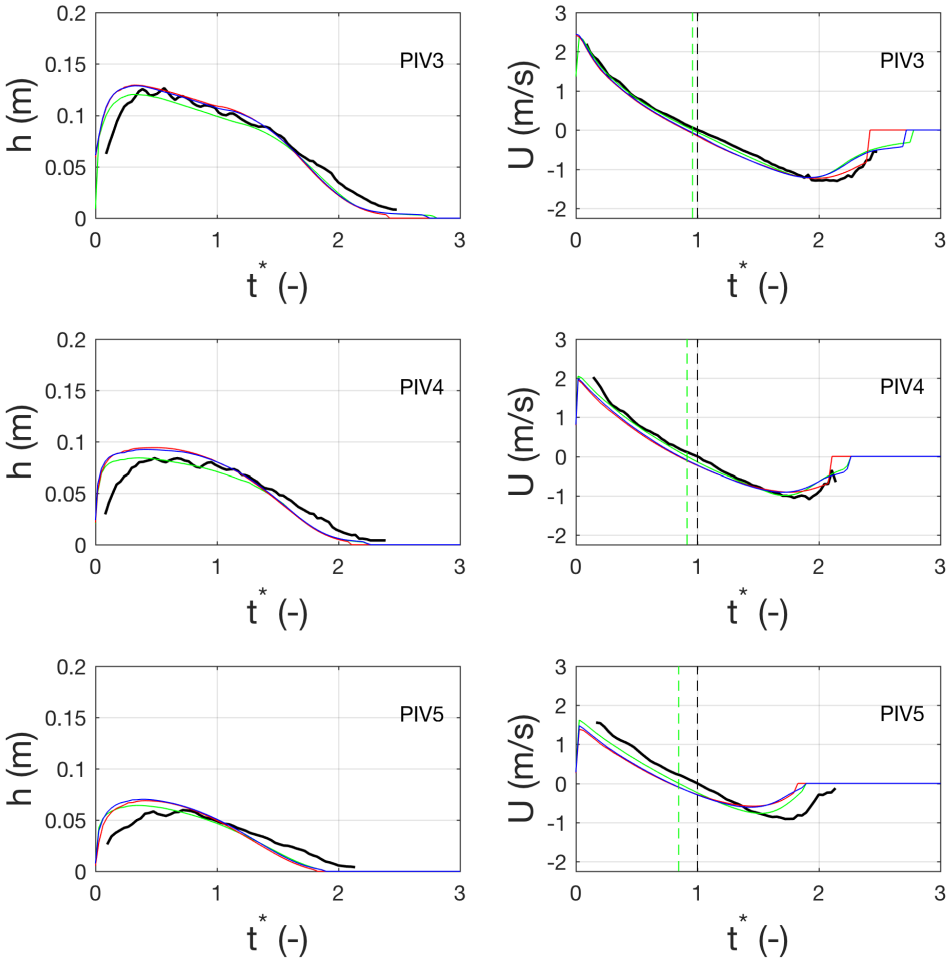

Figure 7: Comparison between numerical and experimental h (left column) and U (right column) at three measurement stations. Experiments (——), numerical model, prediction with the RM (——), numerical prediction with Model 4. t^* for flow reversal in the RM (- - -) and in the experiment (- - -) are also indicated (——), and Model 5 (——).

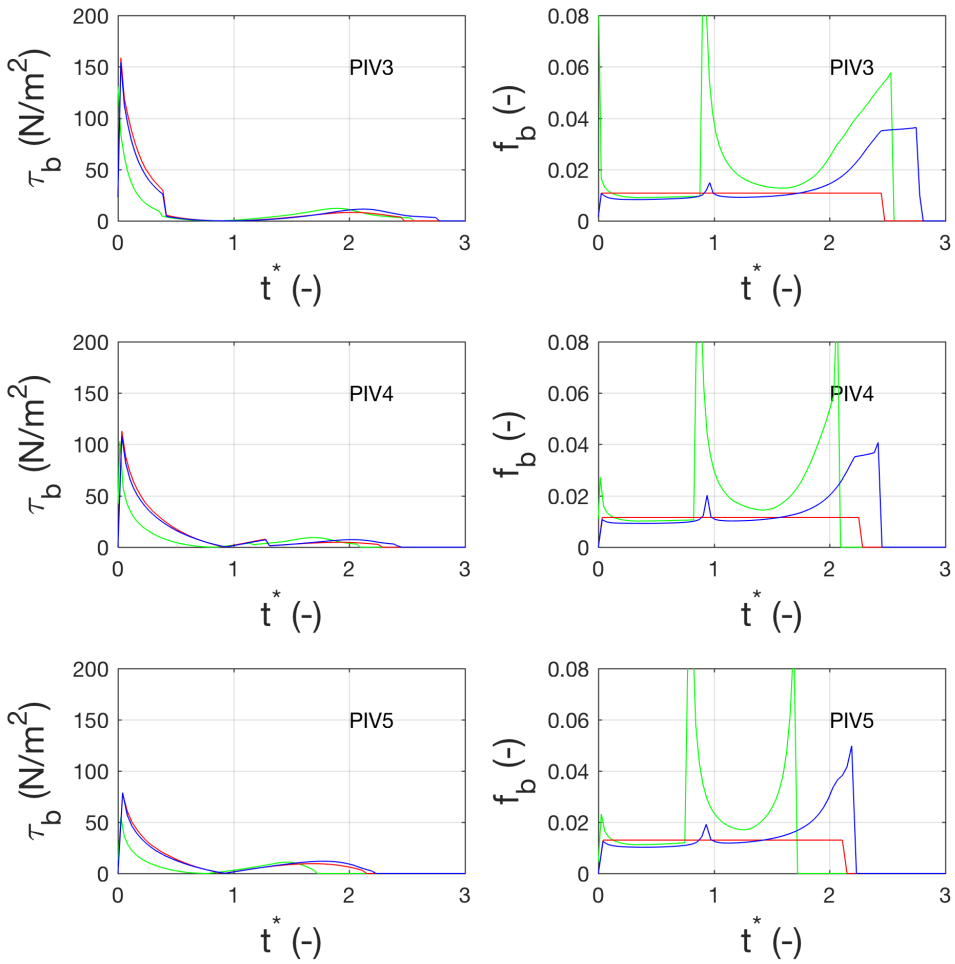

Figure 8: Comparison between numerical $\tau_{b,inf}$ (left column) and f_b (right column) at three measurement stations. Numerical model, prediction of τ_b and back-calculated f_b with the RM (—), numerical prediction with Model 4 (—), and Model 5 (—).

The table shows that the RM, provides more accurate results and the Swart and Colebrook methods show nearly the same ϵ. Analysis of Fig. 7 and Table 4 allows to explain the errors in the prediction. Both h and U are better predicted in the run-up phase, and immediately after flow reversal. At bore arrival the water depth is overestimated in the model, due to the approximation of the NLSWE, which admit only discontinuous bores, while the slope of the free surface is milder in the experiments due to turbulent dissipation, which is not modelled here. In the backwash larger errors occur at later stages and they are larger at $PIV5$, i.e. in the upper swash; this is due to the faster infiltration in modelled backwash with respect to the experiments. Note that the run-up phase is slightly faster in the model with respect to the experiment, i.e. the flow reversal in the model occurs before the reversal in the experiment.

5.4. Sensitivity of sediment transport to τ_b modelling

The analysis of the sensitivity of q_b to the model for the computation of τ_b is carried out by comparing the RM to Model 4 and 5. The results for q_b are shown in Fig 9 and ϵ is show in Table 2) .

The figure reveals that there is relatively little difference in the three models for the run-up phase, while in the backwash these differences are significant. During run-up all tested methods produce similar results in terms of ϵ, with Model 4 performing slightly better than Model 5 at $SED3$. The RM performs better than both Model 4 and 5 in the up-rush, but results among the different models become closer further up the beach. In the backwash the RM results are worse than Model 4 and Model 5 in the upper swash zone. Visual inspection of Fig 9 shows that in the backwash the RM produces better results during the late stage of the backwash, while all methods overestimate q_b at an earlier stage. Overall the RM retains a marginally better ϵ than the two aforementioned models, mainly as a result of better prediction in the uprush. The good performance of Model 4 is not a surprise as the space-varying values of f_b in the Swart Method are directly computed using the measured velocities (see Table 2). The Colebrook formula produces results that are comparable with the momentum integral in the uprush, while in the backwash q_b is lower immediately after flow reversal as a consequence of smaller τ_b predicted.

It is also interesting to compare the volumes of transported sediment (V), obtained by integrating the numerically computed q_b over the duration of the run-up and backwash. Fig. 10 shows V together with the net volume V_{net}, i.e. the difference between V in the uprush and backwash. The numerical results are here compared with the estimates of the volume in O'Donoghue et al. (2016) at each measuring station. For all the options tested for τ_b the largest mismatch in results is found during the run-up phase with the RM method performing significantly better in the upper swash zone. In the backwash all methods perform similarly, with the Swart formula providing the best results at $SED2$. while in the upper part of the beach the RM and Colebrook models provide better results. The qualitative behaviour in the numerical simulation shows some important differences when compared to the experiments. In the numerical uprush volumes do not decay monotonically with distance for $x > 0.6$

m as in the experiment. Volumes increase slightly in the lower part of the beach, up to $SED3$ and then decay. This indicates that the beach is eroding in the lower part and accreting in the mid and upper part during run-up. Note that also in O'Donoghue et al. (2016) the gradient of the transport volumes computed with the MPM formula using the measured velocity (see Fig. 18 of the cited paper) showed very similar characteristics to the present work, above all in the uprush.

5.5. Sensitivity of sediment transport to MPM parameters

Fig 11 shows the results for q_b using four variations of the MPM formula parameters C_s and θ_{cr} (i.e. RM compared to Models 6 to 8). During the run-up phase the model reproduces qualitatively well the evolution in time and space of q_b in all cases. However, quantitative differences are significant; Table 4 shows that ϵ for the RM is significantly lower than that for Model 7b, in which $C_s = 22$. $C_s = 12$ provides ϵ slightly higher than the RM. The test carried out using $\theta_{cr} = 0$ Model 6 shows only marginal differences with the RM in terms of ϵ. Inspection of Fig. 11 reveals that inclusion of a threshold affects the prediction only when the flow velocity is small, i.e. around flow reversal, confirming the findings of Zhu and Dodd (2015), who noted that θ_{cr} has negligible effect in most of the swash cycle.

Table 4: ϵ for the prediction of h and U.

PIV	RM		Model 7a $C_s = 12.0$		Model 7b $C_s = 22.0$		Model 6 $C_s = 8$ $\theta_{cr} = 0.0$		Model 8 $C_{s,u} = 8$ $C_{s,b} = 4.0$		Model 4 Swart		Model 5 Colebrook	
	h	U	h	U	h	U	h	U	h	U	h	U	h	U
PIV 3	0.074	0.0396	0.0756	0.0412	0.0831	0.0452	0.074	0.0394	0.0757	0.0394	0.0906	0.0468	0.0873	0.0485
PIV 4	0.1164	0.0387	0.121	0.0414	0.133	0.0474	0.1164	0.0391	0.115	0.0391	0.1508	0.0620	0.1425	0.0590
PIV 5	0.156	0.1184	0.158	0.120	0.163	0.127	0.1556	0.1184	0.156	0.1184	0.1837	0.161	0.190	0.156

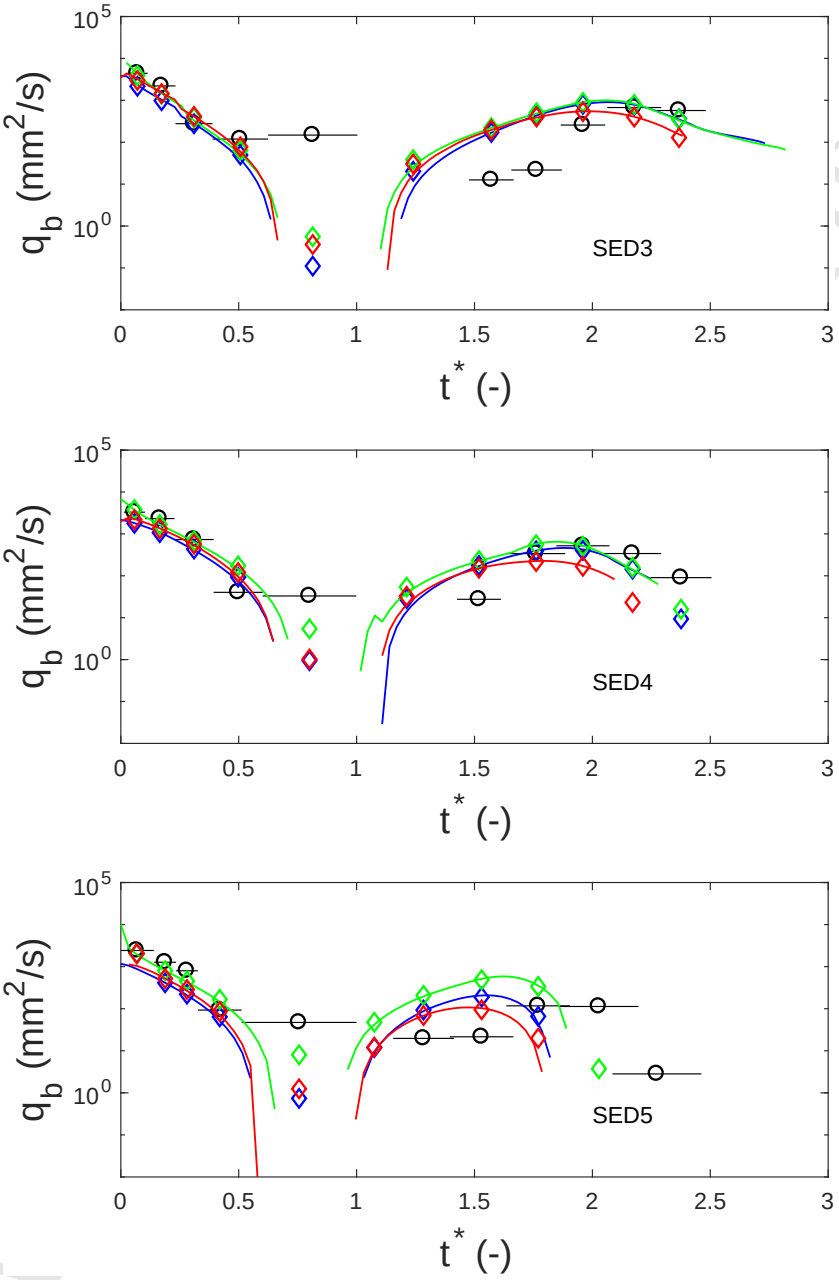

Figure 9: Comparison between measured and modelled q_b at three sediment traps. q_b measured by the traps averaged over the trap release intervals (○). Horizontal black lines: trap release interval. For the numerical results: solid lines, numerical prediction, diamonds averages over the traps release intervals. numerical prediction with the RM (—), numerical prediction with Model 4 (—), and numerical prediction with Model 5 (—).

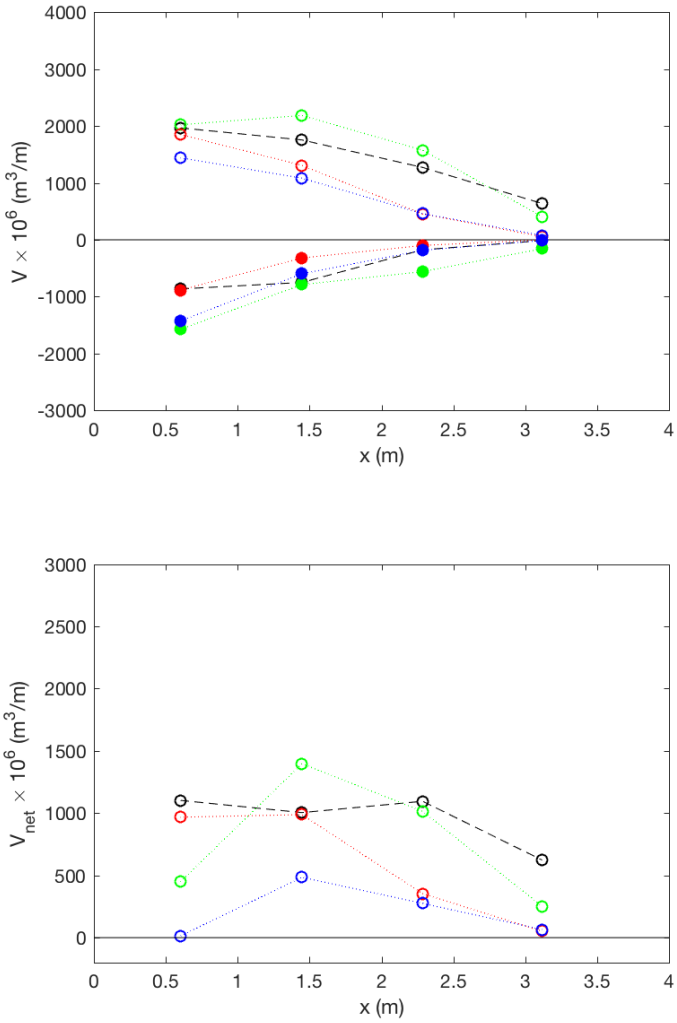

Figure 10: Comparison between measured and modelled V (upper panel, open markers for uprush and shaded markers for downrush) and V_{net} (lower panel) at all the sediment traps. V measured (-⊖-), prediction with the RM (⊖), prediction with Model 4 (⊖), and Model 5 (⊖).

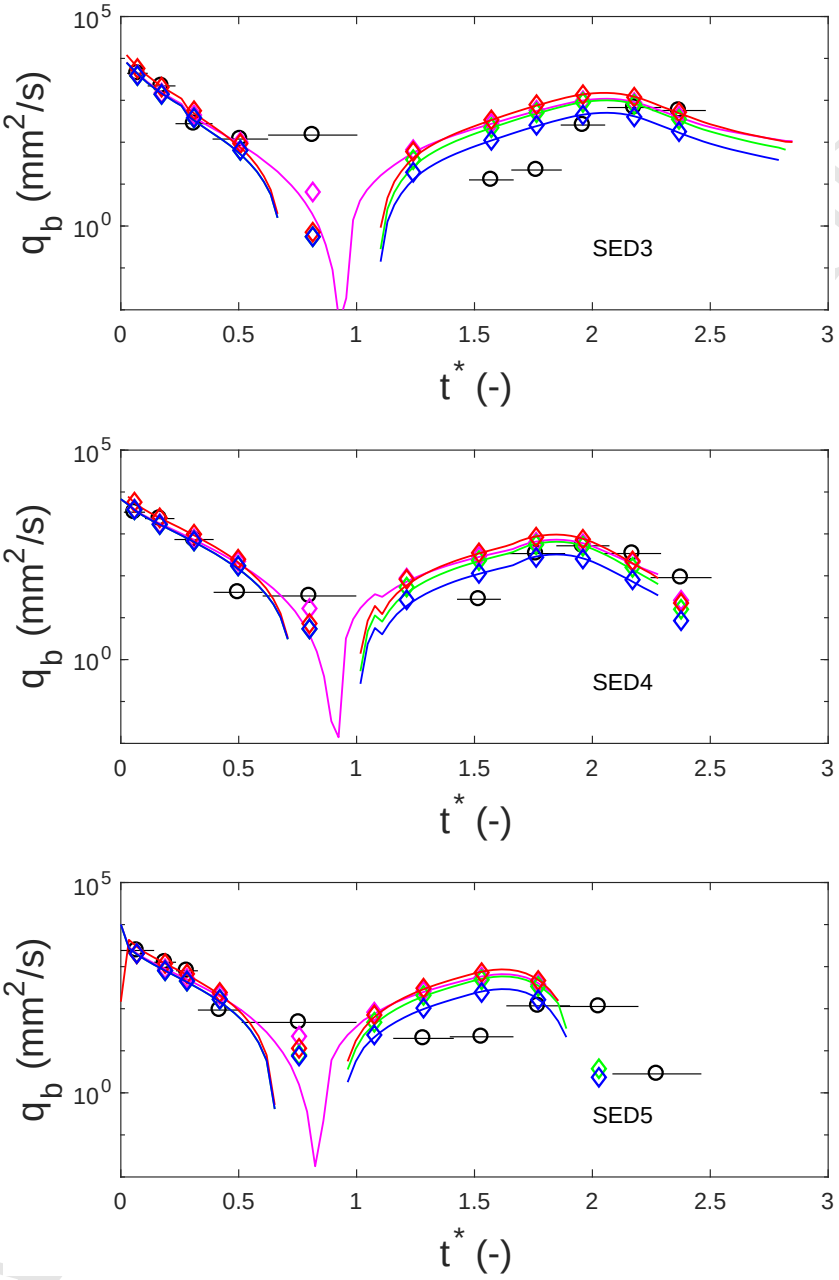

Figure 11: Comparison between measured and modelled q_b at three sediment traps. q_b measured by the traps averaged over the trap release intervals (○). Horizontal black lines: trap release interval. For the numerical results: solid lines, numerical prediction, diamonds averages over the traps release intervals. Numerical prediction with the RM (—), Model 8 ($C_{s,u} = 8.0$, $C_{s,b} = 4.0$) (—), Model 7a ($C_s = 12.0$). (—), and prediction with Model 6 (—).

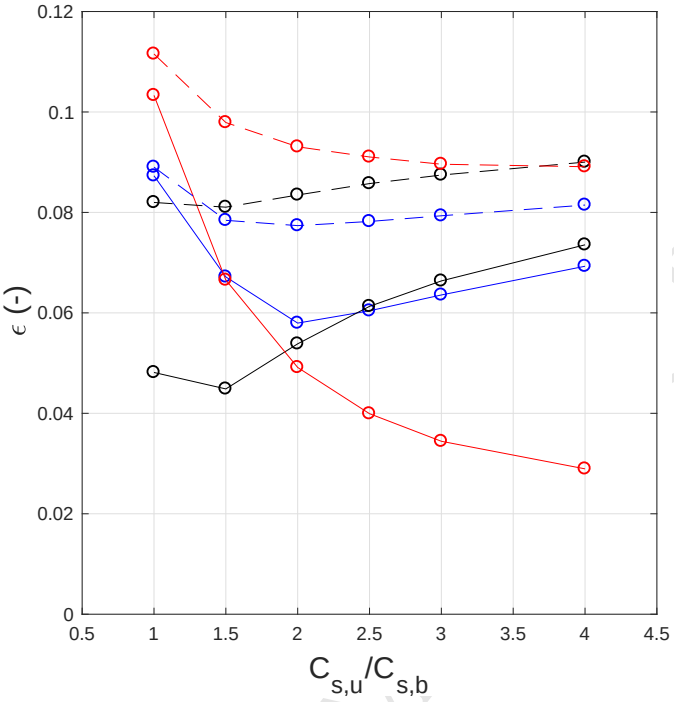

Figure 12: Comparison between ϵ of the predictions of q_b obtained with different values of $C_{s,u}/C_{s.b}$. Solid lines: backwash only. Dashed lines: whole cycle. ϵ for $SED3$ (), ϵ for $SED4$ (), ϵ for $SED5$ ().

With the tested values of C_s the results tend to be less accurate in the backwash than in the uprush, similar to Fig. 9. q_b is overestimated, with values increasing with increasing C_s. A significant improvement in the prediction of the backwash transport is obtained by reducing C_s in the backwash ($C_{s,b}$) with respect to the uprush value ($C_{s,u}$). An analysis of ϵ as the ratio $C_{s,u}/C_{s,b}$ varies is shown in Fig. 12. Here the ratio has been changed keeping $C_{s,u} = 8.0$ and $\theta_{cr} = 0.036$ in all tests. As $C_{s,u}/C_{s,b}$ increases the ϵ in the backwash rapidly decreases at all stations. Correspondingly, ϵ also decreases for the whole cycle. For $SED3$ and $SED4$, ϵ has a minimum $C_{s,u}/C_{s,b} = 1.5$ and 2.0 respectively, while it decreases monotonically for higher values at $SED5$. This is due to the overestimation of q_b during the backwash at $SED5$, which persists even if the sediment transport in the backwash is reduced by a relatively large factor. $C_{s,u}/C_{s,b} = 2.0$ is considered to be the optimal value for the simulations and it is used in the comparison in Table 4. Note that the benefit of reducing the transport in the backwash on ϵ for the whole swash cycle is significant only up to $C_{s,u}/C_{s,b} = 2.0$. Any further increase produces only marginal variations in ϵ. This happens because the benefit of the a lower $C_{s,b}$ is mainly to reduce the modelled q_b after flow reversal, while there is no benefit at later stages of the flow.

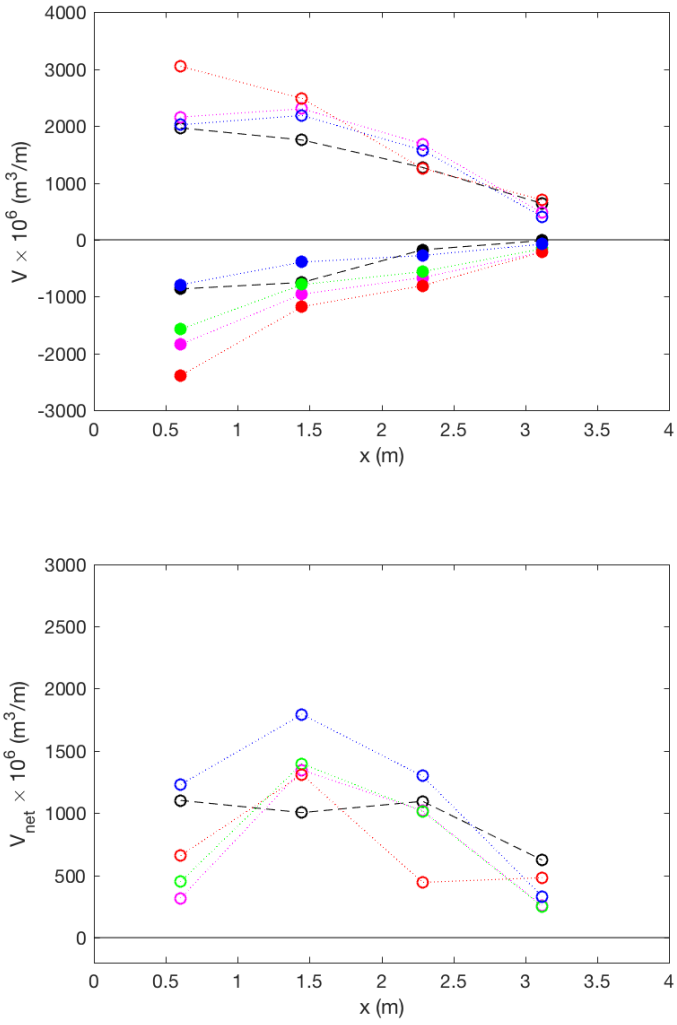

Figure 13: Comparison between measured and modelled V (upper panel, open markers for uprush and shaded markers for downrush) and V_{net} (lower panel) at all the sediment traps. V measured (-⊖-), prediction with the RM (—⊖—), prediction with Model 8 ($C_{s,u} = 8.0$, $C_{s,b} = 4.0$) (—⊖—), prediction with Model 7a ($C_s = 12.0$) (—⊖—), and prediction with Model 6 (—⊖—).

Fig. 13 shows V and V_{net} for the present tests. The results are similar to those

shown for the sensitivity to the model used for τ_b. Best results are shown with C_s variable between uprush and backwash in the lower swash, and C_s constant in the upper swash.

Finally, Model 9, i.e. wth q_b computed with Li et al. (2017), has also been tested. However, results have shown that the sediment transport is never limited to $q_b = hUc_u$, hence the results are the same as the prediction given essentially by MPM formula with $\theta_{cr} = 0$ and τ_b estimated using the Swart method for f_b. and they are not shown in ther paper. Here the order of magnitude of A_s computed using Eq. (23) is 10^{-4} m^2/s. Sensitivity tests on this parameter (not shown in this paper) reveal that q_b becomes limited when $A_s = 8.0 \times 10^{-3}$ m^2/s, which is in the region of bed mobility tested in Li et al. (2017).

5.6. Summary of results

Finally, ϵ for q_b obtained for most of the tests carried out is shown in Table 5. Here it is shown that changing C_s from 8 to 22 produces an increase in ϵ of nearly a factor of 4. The use of the optimal ratio $C_{s,u}/C_{s,b} = 2.0$ produces a reduction in ϵ of an average 30% over the three measuring stations analysed. However, if only the backwash is considered, the reduction is larger for $SED3$ and $SED5$, but ϵ increases for $SED4$. The presence of a threshold, on the other hand, has only a very small effect on ϵ at all measuring sections. As mentioned above, higher values of C_s do not improve the prediction of q_b in either stages of the flow. Finally, using the Swart method produces ϵ that is comparable with the Colebrook estimate of f_b. They both produce generally lower ϵ than the RM during the backwash as a result of the lower $\tau_{b,inf}$ predicted at flow reversal.

5.7. Flow and bed evolution in the swash lens

The model allows a description of the intra-swash flow and bed evolution thus complementing the physical experiments in providing an insight into the intra-swash processes. Here we focus on the description of the predicted bed evolution provided by the RM.

The predicted bed evolution within the swash lens is shown in Fig. 14, where the bed change $\Delta z_b = z_b(t) - z_b(0)$, is plotted. Note that in this case the time is dimensional as the non-dimensionalisation method used for the measurement stations is not suitable for the timestack of the whole swash lens. The large spatial gradient of q_b at the tip, during run-up creates accretion in that region. Erosion is starting to develop during backwash, around the position of the initial shoreline and in the lower swash zone. As velocity decreases behind the uprush tip a region of deposition of sediment is created, consistent with earlier studies (e.g. Zhu et al., 2012). The subsequent backwash erodes much, but not all of this, indicating that this swash event is accretive in mid swash. Note that, since the deposition in the upper part of the beach is very small, the model signal to noise ratio is rather small, making the predicted bed not very smooth.

SED		RM	Model 7a $C_s = 12.0$	Model 7b $C_s = 22.0$	Model 6 $\theta_{cr} = 0.0$	Model 8 $C_{s,u} = 8\ C_{s,b} = 4.0$	Model 4 Swart	Model 5 Colebrook
SED3	Uprush	0.0904	0.129	0.542	0.0774	0.0904	0.145	0.237
	Backwash	0.0872	0.150	0.325	0.0996	0.0604	0.0736	0.0759
	Total	0.0890	0.130	0.457	0.0882	0.0782	0.1211	0.183
SED4	Uprush	0.102	0.303	0.886	0.1054	0.1017	0.1835	0.246
	Backwash	0.0481	0.0878	0.211	0.0570	0.0613	0.0695	0.0393
	Total	0.082	0.231	1.184	0.068	0.0857	0.143	0.183
SED5	Uprush	0.118	0.0781	0.183	0.1047	0.118	0.166	0.186
	Backwash	0.103	0.1549	0.272	0.1211	0.0399	0.032	0.0408
	Total	0.112	0.118	0.228	0.1124	0.0910	0.125	0.140

Table 5: ϵ for the prediction of the averaged q_b.

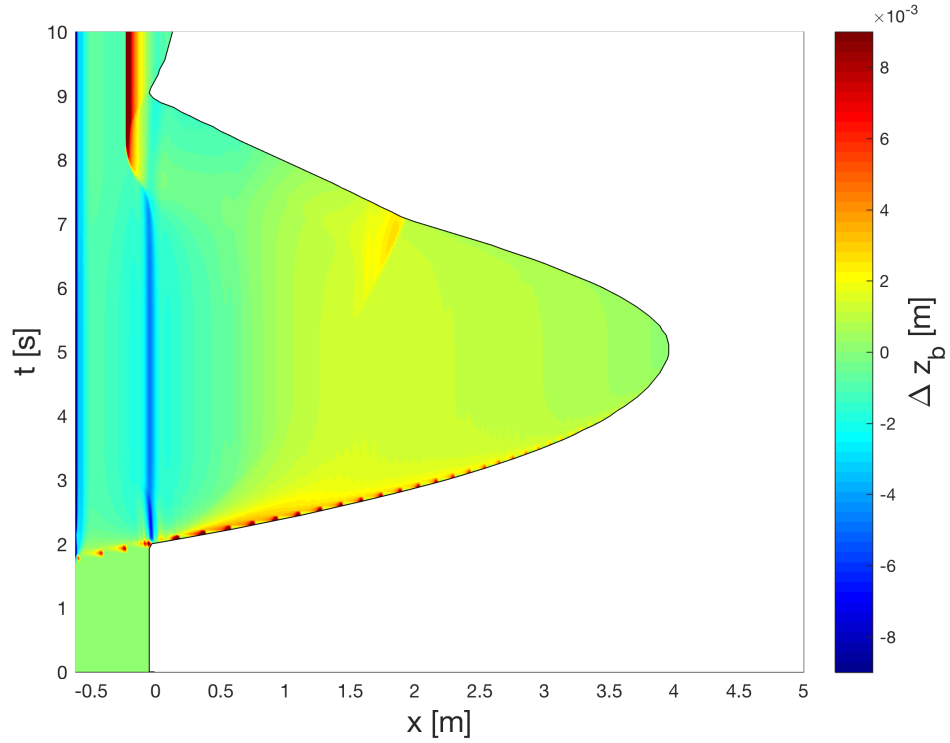

Figure 14: Time stack of the bed change Δz_b during the swash event.

The backwash hydraulic jump progressively develops late in the event, starting from the initial position of the shoreline. In the final stages of the backwash, the sediment step stops moving,

The modelled Δz_b at $PIV3$, $PIV4$ and $PIV5$ is shown in Fig. 15. Here the differences between the lower swash zone and the upper one are clear. At $PIV3$, after accretion during the run-up stage the bed stabilises and at the later stage of the backwash the bed is eroded, resulting in net erosion. At $PIV4$ and $PIV5$, where velocities at the backwash are smaller than in the lower swash, the removal of sediment at the late stage of the backwash is not sufficient to cause net erosion.

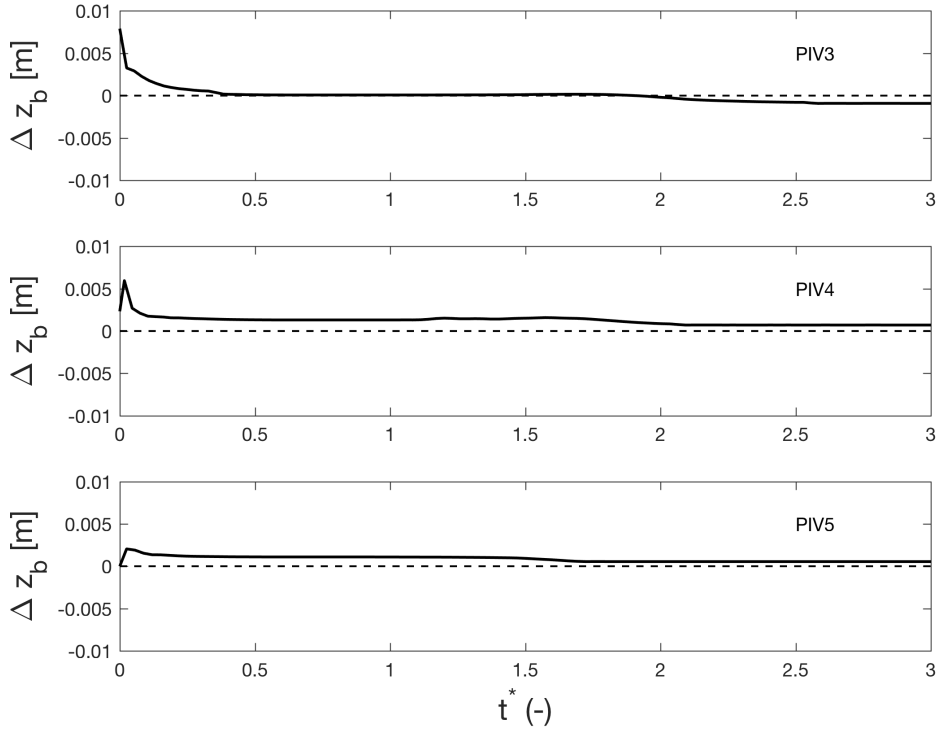

Figure 15: Δz_b (——) at three PIV stations.

6. Discussion and Conclusions

This study presents a sensitivity analysis of the prediction of swash hydrodynamics and sediment transport by testing different options of the MPM formula and different models for the estimation of the bed shear stress. Importantly, we also present a comparison with measurements to assess the accuracy of the approaches.

It is noteworthy that the description of the evolving flow and bed that results from this model shows strong analogy with theoretical idealised cases of single swash events presented in the literature. During the run-up phase the closest theoretical model is the uniform bore discussed in Zhu et al. (2012). In particular, the highest sediment transport found at the tip and the accretion along the swash lens during the run-up are very similar in both the idealised and experimental cases. However, in the backwash, the flow/bed evolution is closer to the case of the solitary wave discussed in Zhu and Dodd (2015). At the late stages of the backwash an hydrodynamic bore and the bed step form just below the original still water level in both cases. As a result, the final bed profile (see Figure 14, in Zhu and Dodd, 2015), for the solitary wave is qualitatively very similar to the case considered in the present work. These results highlights the importance of such idealised cases in understanding the numerical description of more complex swash flows.

It is possible to compare the modelled bed evolution with the experiments of O'Donoghue et al. (2016). The analysis of sediment volumes collected suggested erosion in the lower swash, no change in the mid-swash and net accretion in the upper swash. The qualitative description given by the model is rather different; even though the agreement between modelled and experimental volumes is good, the volume gradients computed using the volumes at the trap location is different. However, with only four locations available, it is questionable whether inferring beach change from the gradients in volumes is of merit. Note also that O'Donoghue et al. (2016) do not make direct measurements of beach change. Accordingly, we tentatively note the discrepancy between the present contribution and the measurements at the most offshore location, but conclude that more experimental work is needed to address this point properly.

A simple model to take into account the effect of the infiltration on the modelling of the bottom shear stress is tested. Although this model is based on a limited number of tests in a u-tube and we have extended it outside the original range of calibration, it provides an estimate of the shear stress in good agreement with the measurements in the uprush. Including this process provides a notionally closer to reality model, as infiltration is a major process in the coarse sand beach. However, it does not give obvious improvement in the accuracy of flow variables (h and U) modelling with respect to disregarding the effect of the infiltration. For example, as Fig. 4 shows, the velocity in the uprush is slightly better modelled in the upper swash zone (e.g. $PIV5$).

All models tested for the shear stress overestimate it immediately after flow

reversal. At a later stage of the backwash, the results are good for $PIV3$ and $PIV5$, while the stress is underestimated at $PIV4$. However, it has to be noted that a direct comparison between the model and experiments is possible for the fixed bed experiments only because it is not possible to apply the log-law in the mobile bed case, hence these results have to be considered with caution. Another reason of the overestimation of $\tau_{b,inf}$ is that here $\tau_{b,inf}/\tau_b = 1.8$ for a significant portions of the swash cycle since, when $w_{inf}/u_f > 0.05$. This is a clear limitation of the extension of the Conley formula, which needs to be addressed in the future research.

An important outcome of the present study is the evidence that the MPM formula predicts the transport during the uprush reasonably well when used with standard values. Large differences in the optimal C_s have been found in seemingly similar case studies. O'Donoghue et al. (2016) found that $C_s = 12$ leads to good accuracy, while Othman et al. (2014) recommended values that are 3 times larger. The possible explanation of this mismatch has already been discussed in O'Donoghue et al. (2016) and it still holds here. While there is still uncertainty in the best value for C_s, this work has given some important indications. However, the MPM formula shows its limited accuracy in the backwash phase. The results strongly suggest that the accuracy of the prediction of q_b increases if C_s is reduced in the backwash with respect to the uprush. Best results are found when this reduction is of a factor 2.0. This reduces the overestimation of q_b obtained when C_s is the same for the uprush and backwash. However, the model still overestimates the transport in the upper swash zone. In general, the model predicts an evolution of q_b in the backwash that is significantly different from the measured one; q_b in the model after flow reversal is one order of magnitude larger than in the measurements. Note that the large mismatch occurs at a stage of the flow (at $1 < t^* < 1.5$ in the case under study) when the prediction of the velocity is accurate.

This study indicates that in the uprush NLSWE coupled with the Exner equation and the MPM formula for sediment transport are able to provide accurate estimate of U, $\tau_{b,inf}$ and, in turn, q_b, although the lack of modelling air-compression in the beach is a limitation for the model. However, the backwash is not equally well modelled. The modelling of this stage needs to be assessed following the different stages of the flow. At flow reversal, although U is accurately modelled, the shear stress is overestimated, in turn q_b is overestimated. It is possible to explain the overestimation of $\tau_{b,inf}$ with the limitations of NLSWE in capturing the vertical structure of the flow, which has been highlighted in Briganti et al. (2011), for the impermeable bed. The lowering of C_s in the backwash only partially mitigates this tendency. In a later stage of the backwash (around $1.5 < t^* < 2$ in the case under study), $\tau_{b,inf}$ is better predicted, however q_b is still overestimated.

It is more complex to explain the mismatch in the subsequent phase of the backwash. Several contributions can be identified. $\tau_{b,inf}$ is not consistently over- or underestimated along the swash lens and the simple infiltration correction used does not capture well the effect of this process. Overestimation of q_b is

also present where $\tau_{b,inf}$ is close to the stress computed from the experimental velocities, indicating that the MPM formula might not capture the complexity of the sediment transport process here.
At a late stage of the backwash the NLSWE solver with the present infiltration model under-predicts U as a consequence of the faster infiltration because air pressure build-up is not considered, hence it is not possible to identify if other physical processes are not well modelled. This mismatch and the lack of experimental data for $\tau_{b,inf}$ on the mobile bed does not allow to assess how the MPM formula is capable of simulating the backwash.

Results of the sensitivity analysis show that the presence of a threshold in the sediment transport formula has been found to have a negligible role in most of the swash cycle as also predicted by Zhu and Dodd (2015). It is also shown that the three models used for τ_b differ mainly in the uprush, where the momentum integral method predicts lower stress. The results for q_b when the RM is compared to Model 4 and 5 suggest that the using momentum integral leads to a marginally more accurate prediction of q_b.
In conclusion, the RM results show marginally more accurate results compared to the other alternatives, in terms of sediment transport as shown in comparing q_b and, in turn, uprush and backwash sediment volumes, in particular in the upper swash zone, as shown in Section 5.4. However, the accuracy of all models in the backwash still needs significant improvement, and that should be a priority for research in swash zone processes. NLSWE modelling is characterised by simple descriptions of physical processes. In this framework the description of backwash processes, by means of more accurate sub-models should be prioritised. In particular, the modelling of air-pressure build up in mobile bed cases, the modelling of the shear stress around flow reversal, an unsteady correction of the effect of infiltration on the shear stress itself, and a more accurate understanding of how well the complexity of the sediment transport in the backwash is captured by the MPM formula, are the next steps in research of modelling intra-swash physical processes. It has to be emphasised that these conclusions are valid for coarse sediment beaches in which bed load is the dominant sediment transport mode. Therefore, there is a need for a similar detailed study on intra-swash sediment transport for bore driven swash on finer sediment beaches.

7. Acknowledgements

This study was supported by the EPSRC through the research project Experimental and Numerical Modelling Study of Swash Zone Hydrodynamics and Sediment Transport (EP/EO10407/1 and EP/E011330/1). Riccardo Briganti was supported by the EPSRC Career Acceleration Fellowship (EP/I004505/1). Prof. Dubravka Pokrajac and Prof. Tom O'Donoghue are acknowledged for the productive discussions throughout the preparation of the manuscript.

Appendix A. Sediment transport derivatives with the integral method

The definition of the TVD function **D** in Eq. (9) requires knowledge of the derivatives $\frac{\partial q_b}{\partial h}$ and $\frac{\partial q_b}{\partial hU}$ in order to find the eigenvalues of the Jacobian matrix of the flux **F** (see Eq. 15 in Briganti et al., 2011). The derivatives can be using the explicit dependence from U when the Chezy formulation of τ_b is used, as done in Briganti et al. (2011). However, this is not the case when the momentum integral method is used. To overcome this difficulty an instantaneous friction factor is defined using the relationship:

$$f_b = \frac{\tau_b}{0.5\rho U^2} \tag{A.1}$$

where τ_b is computed using the momentum integral method. In this way we obtain $\frac{\partial q_b}{\partial h}$ and $\frac{\partial q_b}{\partial hU}$ as:

$$\frac{\partial q_b}{\partial h} = -12 f_b \frac{U^2}{h} \sqrt{\frac{D_{50}}{g\left(s_{rel}-1\right)}} \sqrt{\frac{f_b U^2}{2g\left(s_{rel}-1\right)D_{50}} - \theta_{cr}} \tag{A.2}$$

and:

$$\frac{\partial q_b}{\partial hU} = 12 f_b \frac{U}{h} \sqrt{\frac{D_{50}}{g\left(s_{rel}-1\right)}} \sqrt{\frac{f_b U^2}{2g\left(s_{rel}-1\right)D_{50}} - \theta_{cr}}, \tag{A.3}$$

both for $\theta > \theta_{cr}$.

Appendix B. Computation of u_f

Here we recall the procedure used to compute u_f. Here only a brief description is given, more details on the numerical solution can be found in Briganti et al. (2011). u_f is expressed as:

$$-u_f^2 = \int_{z_0}^{z_0+\delta} \frac{\partial}{\partial t}\left(U_0 - u(x,z,t)\right) dz \tag{B.1}$$

where z is the vertical coordinate, $z_0 = K_n/30$, δ is the thickness of the boundary layer, U_0 is the free stream velocity and $u(x,z,t)$ is the horizontal velocity inside the boundary layer, that is assumed to follow the logarithmic law:

$$u(x,z,t) = \frac{u_f}{\kappa} \ln\left(\frac{z}{z_0}\right) \tag{B.2}$$

where $\kappa = 0.4$ is the von Karman constant. By introducing the non-dimensional variable Z defined as:

$$Z = \ln\left(\frac{\delta + z_0}{z_0}\right) \tag{B.3}$$

it can be shown that the following ordinary differential equation is obtained:

$$\frac{dZ}{dt} = \left[\frac{\kappa^2 U_0}{z_0} - Z\left(e^Z - Z - 1\right)\frac{1}{U_0}\frac{dU_0}{dt}\right] / \left[e^z\left(Z-1\right)+1\right] \tag{B.4}$$

To solve Eq. (B.4) U_0 and its time derivative should be known. U_0 is computed starting from the knowledge of h and U, as shown in Briganti et al. (2011). Note that, in contrast to Briganti et al. (2011), δ is limited to not exceed h.

References

Baldock, T., Nielsen, P., 2010. Discussion of effect of seepage-induced nonhydrostatic pressure distribution on bed-load transport and bed morphodynamicsÓ by Simona Francalanci, Gary Parker, and Luca Solari. ASCE J. Hydraulic Eng. 136, 77–78.

Briganti, R., Dodd, N.and Kelly, D., Pokrajac, D., 2012. An efficient and flexible solver for the simulation of the morphodynamics of fast evolving flows on coarse sediment beaches. International Journal for Numerical Methods in Fluids 69(4), 859–877.

Briganti, R., Dodd, N.and Pokrajac, D., O'Donoghue, T., 2011. Non linear shallow water modelling of bore-driven swash: Description of the bottom boundary layer. Coastal Eng. 58(6), 463–477.

Briganti, R., Torres-Freyermuth, A., Baldock, T., Brocchini, M., Dodd, N., Hsu, T.J., Jiang, Z., Kim, Y., Pintado-Platino, J., Postacchini, M., 2016. Advances in numerical modelling of swash zone dynamics. Coastal Engineering 115, 26–41. doi:10.1016/j.coastaleng.2016.05.001.

Chardón-Maldonado, P., Pintado-Patiño, J.C., Puleo, J.A., 2016. Advances in swash-zone research: Small-scale hydrodynamic and sediment transport processes. Coastal Engineering 115, 8–25.

Conley, D., 1993. Ventilated oscillatory boundary layers. Ph.D. thesis. University of Californi. San Diego, California, U.S.A.

Dodd, N., Stoker, A., Calvete, D., Sriariyawat, A., 2008. On the evolution of beach cusps. J. Fluid Mech. 597, 145–169.

Engelund, F., 1966. Hydraulic resistance of alluvial streams. ASCE J. Hydraulic Eng. 92, 315–326.

Hu, P., Li, W., He, Z., Pahtz, T., Yue, Z., 2015. Well-balanced and flexible morphological modeling of swash hydrodynamics and sediment transport. Coastal Eng. 96, 27 – 37. URL: http://www.sciencedirect.com/science/article/pii/S0378383914001987, doi:http://dx.doi.org/10.1016/j.coastaleng.2014.10.010.

Incelli, G., Dodd, N., Blenkinsopp, C.E., Zhu, F., Briganti, R., 2016. Morphodynamical modelling of field-scale swash events. Coastal Engineering 115, 42–57. URL: www.scopus.com.

Kelly, D.M., Dodd, N., 2009. Floating grid characteristics method for unsteady flow over a mobile bed. Computers and Fluids 38, 899–909.

Kikkert, G., O'Donoghue, T., Pokrajac, D., Dodd, N., 2012. Experimental study of bore-driven swash hydrodynamics on impermeable rough slopes. Coastal Eng. 60, 149 – 166. URL: http://www.sciencedirect.

com/science/article/pii/S0378383911001669, doi:http://dx.doi.org/10.1016/j.coastaleng.2011.09.006.

Kikkert, G., Pokrajac, D., O'Donoghue, T., Steenhauer, K., 2013. Experimental study of bore-driven swash hydrodynamics on permeable rough slopes. Coastal Eng. 79, 42 – 56. URL: http://www.sciencedirect.com/science/article/pii/S0378383913000847, doi:http://dx.doi.org/10.1016/j.coastaleng.2013.04.008.

Li, W., Hu, P., Pähtz, T., He, Z., Cao, Z., 2017. Limitations of empirical sediment transport formulas for shallow water and their consequences for swash zone modelling. Journal of Hydraulic Research 55, 114–120. doi:10.1080/00221686.2016.1212942.

Nielsen, P., 1997. Coastal groundwater dynamics, in: Coastal Dynamics' 97, ASCE. pp. 546–555.

Nielsen, P., Robert, S., Møller-Christiansen, B., Oliva, P., 2001. Infiltration effects on sediment mobility under waves. Coastal Engineering 42, 105–114.

O'Donoghue, T., Kikkert, G.A., Pokrajac, D., Dodd, N., Briganti, R., 2016. Intra-swash hydrodynamics and sediment flux for dambreak swash on coarse-grained beaches. Coastal Engineering 112, 113–130.

Othman, I.K., Baldock, T.E., Callaghan, D.P., 2014. Measurement and modelling of the influence of grain size and pressure gradient on swash uprush sediment transport. Coastal Engineering 83, 1 – 14. URL: http://www.sciencedirect.com/science/article/pii/S0378383913001440, doi:http://dx.doi.org/10.1016/j.coastaleng.2013.09.001.

Pokrajac, D., 2013. Depth-integrated reynolds-averaged navier-stokes equations for shallow flows over rough permeable beds. Journal of Hydraulic Research 51, 597–600.

Postacchini, M., Brocchini, M., Mancinelli, A., Landon, M., 2012. A multi-purpose, intra-wave, shallow water hydro-morphodynamic solver. Advances in Water Resources 38, 13 – 26. URL: http://www.sciencedirect.com/science/article/pii/S0309170811002326, doi:http://dx.doi.org/10.1016/j.advwatres.2011.12.003.

Steenhauer, K., Pokrajac, D., O'Donoghue, T., 2012. Numerical model of swash motion and air entrapment within coarse-grained beaches. Coastal Eng. 64, 113 – 126. URL: http://www.sciencedirect.com/science/article/pii/S0378383912000130, doi:http://dx.doi.org/10.1016/j.coastaleng.2012.01.004.

Steenhauer, K., Pokrajac, D., O'Donoghue, T., Kikkert, G.A., 2011. Subsurface processes generated by bore-driven swash on coarse-grained beaches. Journal of Geophysical Research: Oceans 116, n/a–n/a. URL: http://dx.doi.org/10.1029/2010JC006789, doi:10.1029/2010JC006789.

Turner, I.L., Masselink, G., 1998. Swash infiltration-exfiltration and sediment transport. J. Geophys. Res. 103(C13), 30813–30824.

Zhu, F., Dodd, N., 2013. Net beach change in the swash zone: A numerical investigation. Advances in Water Resources 53, 12–22.

Zhu, F., Dodd, N., 2015. The morphodynamics of a swash event on an erodible beach. J. Fluid Mech. 762, 110 – 140.

Zhu, F., Dodd, N., Briganti, R., 2012. Impact of a uniform bore on an erodible beach. Coastal Eng. 60, 326–333.

Highlights for the manuscript: “Numerical modelling of the flow and bed evolution of a single bore-driven swash event on coarse sediment beaches”

- Single bore-driven swash event are simulated numerically using a fully coupled model to study the sensitivity to the parameters of the Meyer-Peter-Müller formula and the model for the bed shear stress.
- Comparison with laboratory experiments suggests that uprush is well modelled, while in the backwash phase the sediment transport is overestimated.
- An analysis of the performance of the shear stress modelling and of the Meyer-Peter-Müller formula is presented.